2015

IMPROVED SENSITIVITY OF RESONANT MASS SENSOR BASED ON MICRO TILTING PLATE AND MICRO CANTILEVER

Xiaoyu Song
Michigan Technological University

IMPROVED SENSITIVITY OF RESONANT MASS SENSOR BASED ON MICRO TILTING PLATE AND MICRO CANTILEVER

By

Xiaoyu Song

A THESIS

Submitted in partial fulfillment of the requirements for the degree of

MASTER OF SCIENCE

In Mechanical Engineering

MICHIGAN TECHNOLOGICAL UNIVERSITY

2015

This thesis has been approved in partial fulfillment of the requirements for the Degree of MASTER OF SCIENCE in Mechanical Engineering.

Department of Mechanical Engineering-Engineering Mechanics

Thesis Advisor: *Dr. Michele H. Miller*

Committee Member: *Dr. Gregory M. Odegard*

Committee Member: *Dr. Kathleen A. Feigl*

Department Chair: *Dr. William W. Predebon*

Table of Contents

List of Figures

List of Tables

Acknowledgments

My heartfelt and deepest gratitude goes first to my supervisor Dr. Michele H. Miller for her constant instruction and encouragement during my graduate study. Dr. Michele H. Miller walks me through all the difficulties and explains everything in a wise and clear way. She is an inspiration herself, doing research in the diverse field systems and stepping outside the lab to do brilliant and creative things.

Second, I would like to extend my sincere appreciation to my committee members Dr. Gregory M. Odegard and Dr. Kathleen A. Feigl for sharing their time unselfishly and validating of the worthiness of my thesis.

Thirdly, I must thank for my parents, Mr. Minzhi Song and Mrs. Yulan Niu who have supported me mentally, financially. I would also like to thank my wife Mrs. Yaqian Tan for always encourage me during my study abroad.

Abstract

Vapor sensors have been used for many years. Their applications range from detection of toxic gases and dangerous chemicals in industrial environments, the monitoring of landmines and other explosives, to the monitoring of atmospheric conditions. Micro-electrical mechanical systems (MEMS) fabrication technologies provide a way to fabricate sensitive devices. One type of MEMS vapor sensors is based on mass changing detection and the sensors have a functional chemical coating for absorbing the chemical vapor of interest. The principle of the resonant mass sensor is that the resonant frequency will experience a large change due to a small mass of gas vapor change. This thesis is trying to build analytical micro-cantilever and micro-tilting plate models, which can make optimization more efficient. Several objectives need to be accomplished:

(1) Build an analytical model of MEMS resonant mass sensor based on micro-tilting plate with the effects of air damping.
(2) Perform design optimization of micro-tilting plate with a hole in the center.
(3) Build an analytical model of MEMS resonant mass sensor based on micro-cantilever with the effects of air damping.
(4) Perform design optimization of micro-cantilever by COMSOL.

Analytical models of micro-tilting plate with a hole in the center are compared with a COMSOL simulation model and show good agreement. The analytical models have been used to do design optimization that maximizes sensitivity. The micro-cantilever analytical model does not show good agreement with a COMSOL simulation model. To further investigate, the air damping pressures at several points on the micro-cantilever have been compared between analytical model and COMSOL model. The analytical model is inadequate for two reasons. First, the model's boundary condition assumption is not realistic. Second, the deflection shape of the cantilever changes with the hole size, and the model does not account for this. Design optimization of micro-cantilever is done by COMSOL.

CHAPTER I: Introduction

Vapor sensors have been used for many years. Their applications range from detection of toxic gases and dangerous chemicals in industrial environments to the monitoring of landmines and other explosives. Trinitroluene (TNT) [1] leaks out into the surrounding environment when a landmine is buried. Detecting this very small leakage of TNT is an efficient way of detecting the landmines. Most explosive processes release little vapor and it is not possible to detect them effectively by normal methods like a dog's nose. Due to this, the high sensitivity vapor sensors are becoming more necessary.

Micro-electrical mechanical systems (MEMS) fabrication technologies provide a way to fabricate sensitive devices. The vapor sensors have a functional chemical coating for absorbing the chemical vapor of interest. In order to develop the vapor sensor, this thesis is focusing on building the analytical models of resonant mass micro-cantilever and micro-tilting plate sensors with capacitive sensing and capacitive actuation. These analytical models can be used in design optimization of MEMS resonant mass sensor.

The principle of the resonant mass sensor is that the resonant frequency will experience a large change due to a small mass of gas vapor change. The surface of micro-cantilever and micro-tilting plate sensors are coated by chemical materials to absorb chemical vapors, and the sensors are actuated by electrostatic force. The air damping force is an important factor that has the most influences on the sensitivity of resonant mass sensor.

The squeeze film damping model can be built by Finite Element Methods. The numerical models are potentially more accurate, and it can be run in reasonable times given the speed of today's computers. The analytical model can help people to understand the mechanism and physical effects through the model problem. It also can be used to validate the numerical model. Compare to analytical model, the numerical model is also time consuming. Therefore, this thesis is trying to build analytical micro-cantilever and micro-tilting plate models, which can make optimization more efficient.

Because the air damping force has a significant role in sensor sensitivity for resonant mass sensors, how to reduce the air damping force becomes a very important question. There are multiple ways to reduce this force such as decreasing the ambient pressure, decreasing the temperature, increasing the gap between the cantilevers or tilting plates and substrate, and adding a hole in the cantilever or tilting plate. This thesis work kept the ambient pressure, the temperature and the gap as constants during simulation. and focused on optimal shape as way to reduce the air damping. Adding holes in the cantilever and tilting plate will reduce the air damping force, but it also will reduce the electrostatic actuation force and reduce the capacitance for sensing. The lost area, due to holes, will also reduce the area for chemical coating, which absorbs the chemical vapors. These competing effects demonstrate that there will be an optimization hole size in cantilevers and tilting plates.

This thesis has the following objectives:

(1) Build an analytical model of MEMS resonant mass sensors based on micro-tilting plate with the effects of air damping.
(2) Perform design optimization of micro-tilting plate with a hole in the center.
(3) Build an analytical model of MEMS resonant mass sensor based on micro-cantilever with the effects of air damping.
(4) Perform design optimization of micro-cantilever by COMSOL.

CHAPTER II Background

2.1 MEMS Gas Sensors

Micro-electrical mechanical systems (MEMS) fabrication technologies provide a way to fabricate sensitive, low power consumption and inexpensive devices. The MEMS gas sensors are coated by a chemical layer which is used to absorb a gas of interest.

Some MEMS sensors are solid-state devices. They detect the mass change by resistance and temperature change with no moving parts in devices. Zee et al. [2] describes two types of sensor arrays. One design is the silicon substrate coated by an array of 'wells', which is used to absorb the carbon black gas. In the second one, the surface of silicon wafer are coated by an array of high aspect ratio 'wells'. The resistance of the polymer in the well changes when carbon black gas is absorbed. Semancik et al. [3] build a micro hot plate chemical sensor. When carbon monoxide is absorbed by a Pt/SnO_2 sensing film coating, the relationship between conductance and temperature changes. Mesoporous nanocrystalline [4] tin oxide thin film was embedded on a multi-layer structure for MEMS-gas sensors. The resistance changes when hydrogen gas is absorbed by the tin oxide thin film. Then the temperature change is detected by a platinum heater on a ceramic substrate.

MEMS gas sensors have also been developed with moving parts based on micro-cantilever [5]. Instead of measure the properties change of sensor materials, such as resistance and temperature change. This type of MEMS gas sensor measures a mechanical response such as deflection, capacitance change and resonant frequency shift. This kind of sensor is also coated with a material that can absorb the chemical of interest. In the static model, the cantilever will bend on the nanometer scale due to mass added when the sensor layer is exposed to an analyte, a capacitance change between the cantilever and substrate can be detected by electronic circuit measurement. In the dynamic model, the resonant frequency will shift due to chemical vapor mass added. Battiston [6] uses an array of eight silicon cantilevers, they are actuated at their resonance-frequency and the surfaces are coated by polymer. This sensor can detect a variety of chemical substances, such as water, primary alcohol and alkanes. Baselt et al. [7] developed an array of 10 micromachined cantilever beams with 90% palladium- 10% nickel coatings to detect hydrogen.

2.2 Squeeze film damping

The dynamic behavior of a plate is strongly influenced by squeeze film damping effect. Newell [8] observed that when a plate was oscillating near a second surface, the air damping force will be increased due to the squeeze film damping between these two surfaces. When the plate squeeze the gap, the gas in the gap flows out from the venting edge, it damps the displacement motion of the plate. Bao et al. [9] studied the basic Reynolds equations for squeeze film air damping, observed the air damping force consists of two part: the viscous damping force which is related to the moving speed of the plate, and the elastic damping force which is related to the displacement of air compression. He

mentioned that when the plate oscillate at a very slow frequency, the air film will not be compressed and the viscous damping force dominates. When a plate oscillate at a very high frequency, the air will be compressed only with no escape, the viscous damping force will vanish, and the elastic damping force dominates. Bao's squeeze film damping model is only accurate when the border effect neglect. Which means the surface dimensions are much bigger than the air gap. Vermuri et al. [10] observed that the border effect increases the damping force, the damping force increase by 35% when the aspect ratios between the surface length 'a' and gap heigh 'g' is equal to 20. Mohite et al. [11] build a new analytical model to express the stiffness and the damping coefficients of squeeze film damping force based on the perforated back plates. The damping pressure distribution matches very well between analytical model and simulated plates with circular pattern holes.

Kim et al. [12] tested perforated planar microstructures with different size of holes and different numbers of holes. The results show that with the same area ratio of hole areas to plate area, the bigger number of holes, the less the air damping, and the higher quality factor. Pursula et al. [13] simulated a planar gas-damped micro device dynamic behavior under electrostatic loading using finite element method. The various reduced-order and reduced-dimensional methods can make the simulation time more efficient. Nigro et al. [14] compared the analytical model and simulated model by COMSOL Multiphysics for the rigid rectangular plate with squeeze film damping phenomenon. The analytical models with high holes ratio and high number holes are effective, but its do not always model realistic very well. The simulated results are matches the experiment result very well, therefore simulate approach are more competitive than analytical methods. Li et al. [15] build an analytical model of circular perforated microplates using a modified Reynolds equation, the viscous damping and spring coefficient of squeeze film damping equation have been found. The analytical model and finite element method results matched very well during the smaller perforation ratios ($2r_0/l_0 \leq 0.6$). Li et al. [16] present an analytical model with the squeeze film damping based on perforated torsion microplates. The analytical model give good results for the devices with $l_h/l_p \leq 0.6$.

2.3 Definition of Sensitivity

The vapor sensor is covered by a chemical coating, which is used to absorb the particular chemical vapor molecules. The design optimization of a resonant mass sensor requires a metric to describe how the frequency response changes due to the mass change caused by chemical absorption. There are multiple ways to characterize sensitivity. One common measure for sensitivity is the shift of resonant frequency caused by a mass change due to chemical absorption [17]. This can be expressed as $S = \frac{\Delta f_r}{\Delta m}$. However, for a damped system without a sharp resonant peak, the resonant frequency shift is hard to detect. Thus, using only the parameter 'S' is not a good way to define the sensitivity. Another important factor is detectability. Quality factor Q characterizes detectability, which is inversely related to damping. [18]. Q is the ratio of resonant frequency without chemical absorption to the

bandwidth, and can be expressed as $Q = \frac{f_r}{\Delta f}$, where Δf is the frequencies shifts at which the amplitude of frequency response is $\frac{\sqrt{2}}{2}$ of the amplitude at resonant frequency. Another approach to define the performance of a resonant mass sensor is to calculate the root mean square deviation (RMSD) [19] between the frequency responses with and without chemical absorption. It can be expressed as $\text{RMSD}\% = \sqrt{\frac{\sum_{i=1}^{N}(M_i^1 - M_i^0)^2}{\sum_{i=1}^{N}(M_i^0)^2}}$. This approach needs a range of frequency response points. In order to simplify the calculation, Miller and Li [20] defined a new measure Qs, which is to calculate the root mean square deviation for just two frequencies: the resonant frequencies with and without chemical absorption. This is expressed as below:

$$Q_S = \sqrt{\frac{(M_{ab}^r - M_{no})^2 + (M_{no}^r - M_{ab})^2}{(M_{no})^2 + (M_{ab})^2}} \times 100\% \tag{2.1}$$

Where M_{ab}^r and M_{no}^r are the magnitude ratio at the resonant frequencies of the absorbed mass system and without absorb system, respectively. Figure 2.1 shows the frequency responses for two different systems with and without absorbed chemical vapor mass. It also shows the parameters in the previous equation.

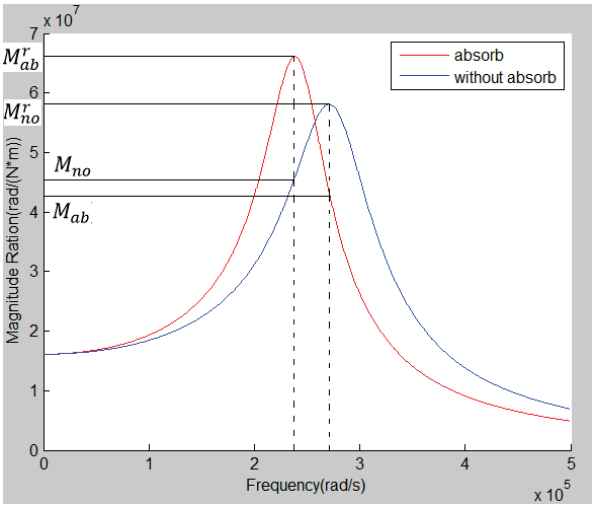

Figure 2.1: The parameter definitions of Qs

Miller and Li [21] compared Qs and RMS for a range of frequency points and found-the shape of these two parameter plots to be very close. Also, in a comparison of Qs, S and Q, the results show that S does not relate to the damping coefficient. Since Qs considers both the sensitivity, and the detectability, this thesis uses this parameter Qs to do the design optimization.

2.4 Analytical models

Darling, et al. [22] developed an analytical model of squeeze film damping with different venting boundary conditions based on a Reynolds equation and Green's function approach. When two plates move toward each other, the laminar flow of a viscous fluid in the gap will be flows out, and the local pressure within the gap can be expressed by Reynolds lubrication equation. If the displacement of the plate is much smaller than the gap, then the Reynolds lubrication equation can be linearized and expressed as:

$$\nabla^2 P - \alpha^2 \frac{\partial P}{\partial t} = \alpha^2 \eta \frac{\partial H}{\partial t} \tag{2.2}$$

Where $P = \frac{\delta p}{P_a}$ is the normalized local pressure variation, P_a is the ambient pressure. $H = \frac{\delta h}{h_0}$ is the normalized local gap variation. h_0 is the nominal gap. $\alpha^2 = \frac{12\mu}{\eta {h_0}^2 P_a}$ is a constant. μ is the viscosity of fluid, and η=1 for an isothermal process. The solution of this equation e can be expressed as an integral of the Green's function over the source points.

$$P(r,t) = \int_0^t \int_{V_0} G(r,t|r_0,t_0) * \rho(r_0,t_0) dr_0 dt_0 \tag{2.3}$$

Here, $\rho(r_0,t_0) = \frac{-\alpha^2 \eta}{4\pi} \frac{\partial H}{\partial t_0}$, where $H(x_0,y_0,t_0)$ is a function of normalized displacement and can be expressed as $H' e^{jwt_0}$, then times a coefficient of plate deflection function. Such as 1 for the rigid flat plate, $\frac{x^2}{L^2}$ for the regular cantilever and $\frac{2x}{L}$ for the regular tilting plate about y axis. The Green's function is expressed as:

$$G(r,t|r_0,t_0) = \frac{4\pi}{\alpha^2} \Theta(t-t_0) * \sum_{m,n} \exp\left(\frac{-{k_{mn}}^2 (t-t_0)}{\alpha^2}\right) u_{mn}(r) {u_{mn}}^*(r_0) \tag{2.4}$$

Where k_{mn} is the eigenvalue and u_{mn} is the eigenfunction, calculated from the two-dimensional scalar Helmholtz equation, $\nabla^2 u_{mn} + k_{mn}^2 u_{mn} = 0$, The eigenvalues and eigenfunctions change according to different boundary conditions. Finally, $\Theta(t-t_0)$ is the unit step function. The net reaction force of the squeeze film damping on the plate can be calculated by integrating the pressure over the plate area.

Darling, et al. derive analytical models of squeeze film damping for rigid rectangular plate with six venting boundary conditions, all edges vented, one edges closed, two adjacent edges closed, two opposite edge closed, three edges closed, and all edges closed. Subsequently, Miller and Li [21] build an analytical model for a square rigid flat plate with a hole in the center. This model contains four elements of two adjacent edges closed and four elements of two opposite edges closed. In the situation of the ambient pressure is one atmospheric pressure, gap underneath the plate is 4 μm, stiffness of supporting legs is

$50N/m$, and material damping is $1 \times 10^{-5}Ns/m$. The best square hole size for $200\ \mu m\ \times$ $200\ \mu m$ square rigid flat plate is $160\ \mu m \times 160\ \mu m$ for design optimization.

CHAPTER III: Resonant Mass Sensor Design Based on Tilting Plate

3.1 Tilting plate about the *y* axis

Tilting plate structure is one kind of ideal resonant mass sensor models, and it is strongly impacted by squeeze film compressive damping. This section derives an analytical squeeze film damping model of a tilting plate about the y axis according to the Green's function approach following the derivation of Darling [22]. In order to build the tilting plate model, a rigid rectangular plate is connected by two leg beams and it's considered as a fixed-free torsional beam. The gap between the plate and the substrate is uniformly held as a constant when the plate is not oscilatting. Design optimization of tilting plate can be done by finite element analysis, but it has to build so many simulative models and it's a time consuming task. The analytical model would make the optimization more effective.

3.1.1 Analytical model of tilting plate without holes

The domain of the tilting plate is $-\frac{a}{2} < x < \frac{a}{2}$ and $-\frac{b}{2} < x < \frac{b}{2}$, corresponding to a rectangular plate with length a and width b. The four edges are assumed to have ideal venting, and the plate tilts about its midline along the *y* axis. The plate can be represented with a model as shown in Figure 3.1.

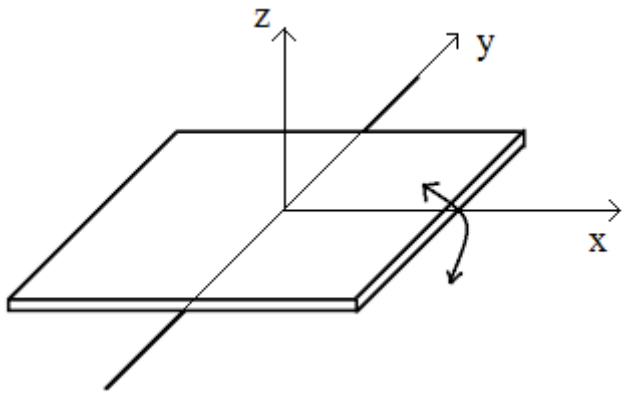

Figure 3.1: The tilting plate about *y* axis

For this plate, the normalized displacement is approximated as:

$$H(x, y, t) = H' \frac{2x}{a} e^{j\omega t} \tag{3.1}$$

Where H' is the normalized magnitude of displacement in direction of z, $H' = \frac{x}{h_0}$, and where h_0 is the tip displacement at $x = -\frac{a}{2}$ or $x = \frac{a}{2}$. The maximum angle of rotation can be described as:

$$\theta_{max} = tan^{-1}(\frac{2h_o H'}{a}) \tag{3.2}$$

Because the boundary condition is ideal venting on four edges in this situation, the eigenfunctions u_{mn} and eigenvalues k_{mn} are calculated by the two-dimensional scalar Helmholtz equation and can described as:

$$u_{mn}(x,y) = \sqrt{\frac{4}{ab}} \begin{matrix}\cos \\ sin\end{matrix} \frac{m\pi}{a}(x) \begin{matrix}\cos \\ sin\end{matrix} \frac{n\pi}{b}(y) \tag{3.3}$$

Where *cos* is used for $m, n = \{1, 3, 5 \ldots.\}$ and *sin* is used for $m, n = \{2, 4, 6 \ldots.\}$; the corresponding eigenvalues are:

$$k_{mn} = \frac{m^2\pi^2}{a^2} + \frac{n^2\pi^2}{b^2} \tag{3.4}$$

The normalized pressure can be calculated by the integral equation shown in Darling's paper:

$$P(x,y,t) = \sum_{\substack{m=even \\ n=odd}} \frac{16(-1)^{m/2-1}(-1)^{(n-1)/2}}{\pi^2 mn} \frac{-j\omega H' e^{j\omega t}}{j\omega + k^2_{mn}/a^2} sin\frac{m\pi x}{a} cos\frac{n\pi y}{b} \tag{3.5}$$

$m = \{2, 4, 6 \ldots.\}$ and $n = \{1, 3, 5 \ldots.\}$. The torque is calculated by force times the distance, so the normalized restoring torque can be described as:

$$\begin{aligned}\tau(t) &= P_a \int_{-a/2}^{+a/2} \int_{-b/2}^{+b/2} xP(x,y,t)dxdy \\ &= \frac{a^2 bP_a}{2} \sum_{\substack{m=even \\ n=odd}} \frac{64}{\pi^4 m^2 n^2} \frac{-jwH' e^{j\omega t}}{j\omega + k^2_{mn}/a^2}\end{aligned} \tag{3.6}$$

P_a is the ambient pressure.

According to the Hooke's law,

$$\tau = Fd = k\theta \tag{3.7}$$

The rotational angle θ is calculated by the maximum displacement at the tip divided by half of the length of the tilting plate, $\theta = \frac{V_{tip}}{a/2}$. The torque can then be rewritten as:

$$\begin{aligned}\frac{\tau(t)}{abP_a} &= \sum_{\substack{m=even \\ n=odd}} \frac{64}{\pi^4 m^2 n^2} \frac{-j\omega e^{j\omega t}}{j\omega + k^2_{mn}/a^2} \frac{a}{2} H' \\ &= \sum_{\substack{m=even \\ n=odd}} \frac{64}{\pi^4 m^2 n^2} \frac{-j\omega e^{j\omega t}}{j\omega + k^2_{mn}/a^2} \frac{a}{2} \frac{V_{tip}}{h_0} \\ &= \sum_{\substack{m=even \\ n=odd}} \frac{64}{h_0 \pi^4 m^2 n^2} \frac{-j\omega e^{j\omega t}}{j\omega + k^2_{mn}/a^2} (\frac{a}{2})^2 \frac{V_{tip}}{\frac{a}{2}} \\ &= \sum_{\substack{m=even \\ n=odd}} \frac{64}{h_0 \pi^4 m^2 n^2} \frac{-j\omega e^{j\omega t}}{j\omega + k^2_{mn}/a^2} (\frac{a}{2})^2 \theta\end{aligned} \tag{3.8}$$

The normalized restoring torque function can be used to find stiffness and damping of air. The real part value is the spring component (k) of air, which is calculated by the reaction torque divided by the rotational angle (θ). The imaginary part value is the damping component (b) of air, which can be calculated by the reaction torque divided by the rotation angle velocity ($\omega\theta$):

$$k_{air} = Re(\sum_{\substack{m=even \\ n=odd}} \frac{64}{h_0\pi^4 m^2 n^2} \frac{-j\omega e^{j\omega t}}{j\omega + \frac{k^2 mn}{a^2}} \left(\frac{a}{2}\right)^2 abP_a) \tag{3.9}$$

$$b_{air} = Im(\sum_{\substack{m=even \\ n=odd}} \frac{64}{h_0\pi^4 m^2 n^2} \frac{-j\omega e^{j\omega t}}{j\omega + \frac{k^2 mn}{a^2}} \left(\frac{a}{2}\right)^2 abP_a) \tag{3.10}$$

Figure 3.2 is showing the free body diagram of tilting plate about y axis.

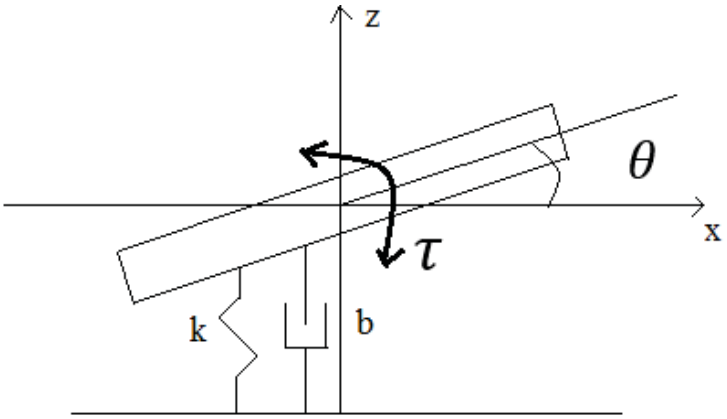

Figure 3.2: Free body diagram of tilting plate

According to the Newton's second law and the free body diagram, the equation of motion for a second order rotational system is:

$$I\ddot{\theta}(t) + b(\omega)\dot{\theta}(t) + k(\omega)\theta(t) = \tau(t) \tag{3.11}$$

Where b is the damping coefficient of air, and k is the sum of stiffness of material and air. $k = k_{flex} + k_{air}$. I is the mass moment of inertia, which can be calculated by:

$$I = \frac{1}{12}ma^2 \tag{3.12}$$

The magnitude ratio function can be expressed as:

$$\frac{\theta(t)}{\tau(t)} = \sqrt{\frac{1}{\left((k_{flex}+k_{air}(\omega)) - I\times\omega(t)^2\right)^2 + (b_{air}(\omega)\times\omega(t))^2}} \tag{3.13}$$

Then, the analytical frequency response of the tilting plate can be calculated with MATLAB by using the parameters shown in Table 3. 1.

Table 3. 1: Parameters used in both analytical and simulated tilting plate models

Pa	101000 Pa
$\mu_{effective}$	1.862×10^{-5} Pa.s
L	200 μm
W	200 μm
t	3 μm
ρ	2330 kg/m^3
m	2.796×10^{-10} kg
g_0	4 μm
k_{flex}	$2 \times 10^{-7} Nm/rads$

Simulated model in COMSOL MULTIPHYSICS

The analytical model was validated using a COMSOL model. The steps for creating a COMSOL model and comparing its results with the analytical model were as follows:

1. Sketch a tilting plate in COMSOL MULTIPHYSICS as show in Figure 3.3 using the parameters in Table 3.1.
2. Choose the solid mechanics physics and time dependent model.
3. According to a COMSOL test, two 30 um × 3 um × 3 um silicon beams which act as a folded leg can supply a torsional stiffness (k_{flex}) of $2 \times 10^{-7} Nm/rads$. Set the density of the two tiny beams to $1e-3\ kg/m^3$ so that the mass of the two beams is small, it will thus have minimal influence on the mass moment of inertia of the tilting plate.
4. Thin-film damping is put on the bottom surface of the plate. The gap is 4 um and the ambient pressure is 1 atmospheric pressure. The original viscosity of air is 22.6×10^{-6} *Pa-s* in the room temperature which is 293.15 *K*.
5. Make the silicon tilting plate as a rigid plate so that there is no deformation during the motion.
6. Apply two opposite sinusoid forces 1×10^{-2}×*sin(w×t) N* at the connection points between tilting plate and legs, this two opposite time dependent forces can make the plate tilt about two legs. Make sure the deflection will be in the elastic region.
7. Collect each maximum displacement value of the free edge in different frequencies. The simulated magnitude ratio is equal to the angle θ divided by the torque τ.

8. Compare the frequency responses of the analytical and COMSOL models.

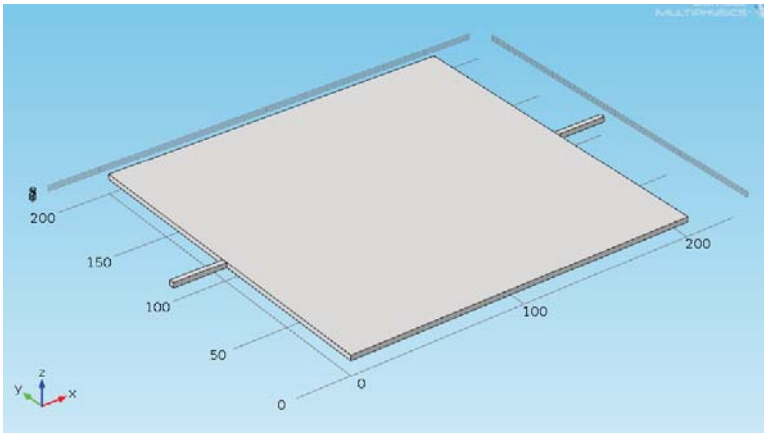

Figure 3.3: The tilting plate model build in COMSOL

Figure 3.4 shows the mesh for the COMSOL model. The 'Free Tetrahedral' element can be used. The element shape is a triangle and it has three node. According to the test, mesh dimension of 'Coarse' is already reached the mesh optimization, and the mesh at the corners are well connected. A finer mesh is not necessary and the coarse mesh will save the running time. The number of elements of this model is more than 5000, and it will take almost 10-15 minutes to get one frequency response point.

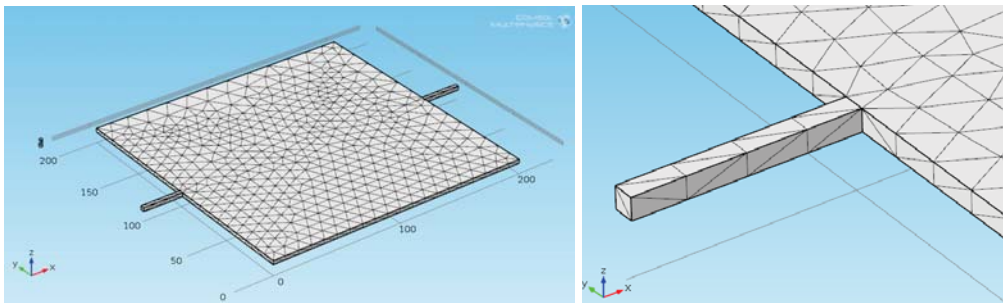

Figure 3.4: Mesh of tilting plate

Figure 3.5 is showing the comparison of frequency response. For the analytical results, the maximum Magnitude Ratio is 1.023e7 *rad/N-m*, and the resonant frequency is 4.38e5 *rad/s*. For the simulated frequency response, the maximum Magnitude Ratio is 1.07 *rad/N-m*, and the resonant frequency is 4.37e5 *rad/s*. For this model, the analytical result is pretty close to the simulation result. The analytical model determines this result in just 1 minute, and each point of simulative result need at least 10 minutes running time. This can demonstrate the efficiency of the analytical model.

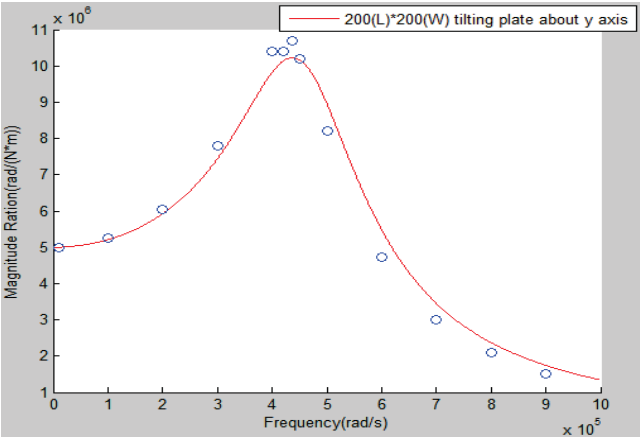

Figure 3.5: The frequency response of tilting plate about y axis

Figure 3.6 shows additional comparisons for different sized tilting plates. The results indicate that the analytical model matches the simulation very well. As mentioned before, the air damping will influence the magnitude ratio; the magnitude ratio at the resonant frequency increases when the air damping decreases. Figure 3.6 shows that the smaller tilting plates have less air damping. However, a large plate is better for actuation, sensing and also absorbing the chemical materials. Therefore, adding a hole in tilting plate is a more efficient way to reduce air damping.

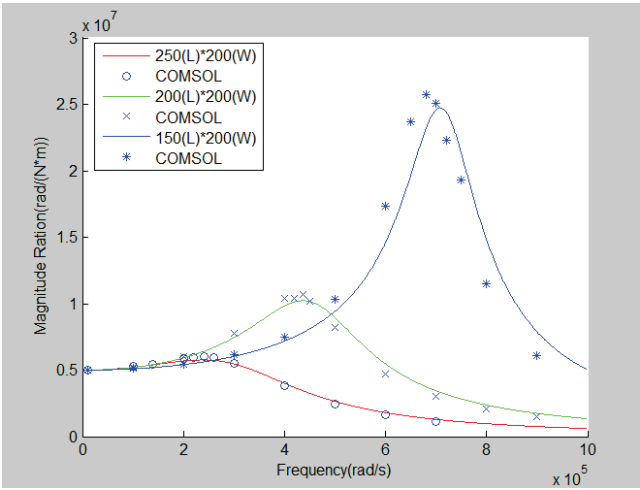

Figure3.6: Model comparison for different sizes of plates that tilt about y axis

3.1.2 Tilting plate about the y axis with a hole in the center

Adding a hole in the center of tilting plate can reduce the air damping and thus increase the Q value significantly. Different hole sizes are tested during the design process. The models in Darling's paper [22], there are five basic boundary conditions with different venting edges: all edges vented, one edge closed, two edges closed, three edges closed, and all edges closed. All five analytical equations are derived based on Green's function and linearized Reynolds equations.

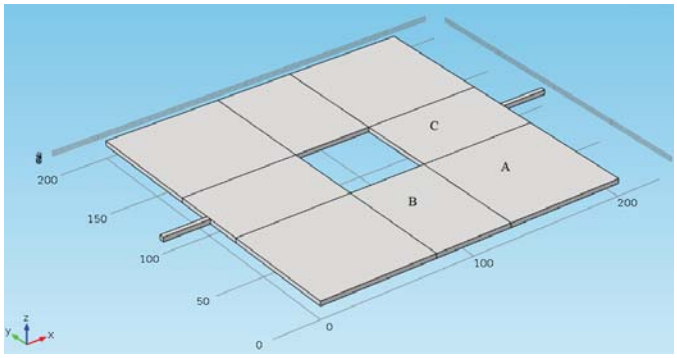

Figure 3.7: Tilting plate about y axis with a hole in the center

Figure 3.7 is showing a square tilting plate with a hole in the center. The tilting plate is divided into eight kinds of rectangular plates with three different boundary conditions. Element 'A' has two adjacent edges closed, element 'B' has two opposite edges closed along the y axis, and element 'C' has two opposite edges closed along the *x* axis. The analytical equations of each element can be derived.

The square plate in Fig 3.7 has length "a" and it tilts about the *y* axis. The maximum displacement in *z* direction occurs at $x=\pm\frac{a}{2}$. The normalized displacement of the plate can be described as

$$H(x,y,t) = H'\frac{2x}{a}e^{jwt} \tag{3.14}$$

Where H' is the normalized maximum displacement at $x=\pm\frac{a}{2}$.

3.1.2.1 Element 'A' with two adjacent edges closed

The domain of the compressed area of element 'A' in Figure 3.7 has two adjacent edges closed. To derive the analytical equation of element 'A', begin with the equation for the regular tilting plate with two adjacent edges closed. The integral procedure is the same as the tilting plate shown above; the only things changed are the eigenfunctions and eigenvalues corresponding to different boundary conditions. The boundaries of 'A' are taken to be $-\frac{a}{2} < x < \frac{a}{2}$, $-\frac{b}{2} < y < \frac{b}{2}$, corresponding to a rectangular plate of dimensions $a \times b$. For the two closed adjacent edges, The boundary conditions are expressed as $\frac{\partial P}{\partial x} = 0$

on $x = -\frac{a}{2}$, and $\frac{\partial P}{\partial y} = 0$ on $y = -\frac{b}{2}$, with ideal venting $P=0$ along the remaining two edges of $x = \frac{a}{2}$ and $y = \frac{b}{2}$. The eigenfunctions are:

$$u_{mn}(x,y) = \sqrt{\frac{4}{ab}} \cos\frac{m\pi}{2a}\left(x + \frac{a}{2}\right) \cos\frac{n\pi}{2b}\left(y + \frac{b}{2}\right) \tag{3.15}$$

Where $m, n = \{1, 3, 5 \ldots\ldots\}$. The corresponding eigenvalues are

$$k_{mn} = \frac{m^2\pi^2}{4a^2} + \frac{n^2\pi^2}{4b^2} \tag{3.16}$$

The restoring torque on the plate can be computed as:

$$\tau(t) = \sum_{\substack{m=odd \\ n=odd}} P_a \frac{-j\omega H' e^{j\omega t}}{j\omega + k^2 mn/a^2} \frac{128\text{ab}}{a\pi^6 m^4 n^2} \left(\frac{\pi\text{m}a}{2}(-1)^{\frac{m-1}{2}} - 2\text{a}\right)^2 \tag{3.17}$$

The real part is the spring stiffness (k) of air, and the imaginary part value is the damping (b) of air. The stiffness of air underneath tilting plate is the spring component of the reaction force divided by the tip displacement.

$$k_{spring} = \tau(t)/H'$$

$$= Re\left[\sum_{\substack{m=odd \\ n=odd}} P_a \frac{-j\omega e^{j\omega t}}{j\omega + k^2 mn/a^2} \frac{128\text{ab}}{a\pi^6 m^4 n^2} \left(\frac{\pi\text{m}a}{2}(-1)^{\frac{m-1}{2}} - 2\text{a}\right)^2\right] \tag{3.18}$$

Similarly, the damping coefficient of air underneath tilting plate can be determined from the damping component of the reaction force divided by the tip velocity:

$$b_{damping} = \tau(t)/v$$

$$= Im\left[\sum_{\substack{m=odd \\ n=odd}} P_a \frac{-je^{j\omega t}}{j\omega + k^2 mn/a^2} \frac{128\text{ab}}{a\pi^6 m^4 n^2} \left(\frac{\pi\text{m}a}{2}(-1)^{\frac{m-1}{2}} - 2\text{a}\right)^2\right] \tag{3.19}$$

Using the same analytical magnitude ratio function shown in the regular tilting plate, it can be expressed as:

$$\frac{\theta(t)}{\tau(t)} = \sqrt{\frac{1}{\left(\left(k_{flex} + k_{air}(\omega)\right) - I\times\omega(t)^2\right)^2 + \left(b_{air}(\omega)\times\omega(t)\right)^2}} \tag{3.20}$$

Simulated model in COMSOL

The procedure is similar to that for the regular tilting plate. The procedure begins with sketching a tilting plate in COMSOL MULTIPHYSICS by using the parameters shown in Table 3.1. Because of the two adjacent edges closed boundary condition in analytical equation, a "wall" needs to be created at these edges which blocks any air from crossing. It simulates the same boundary condition as in the analytical model. Next, apply a sinusoidal torque input and collect the maximum displacement value of the free edge. Repeat this for different input frequencies. The simulated magnitude ratio is equal to the angle θ divided by the torque τ.

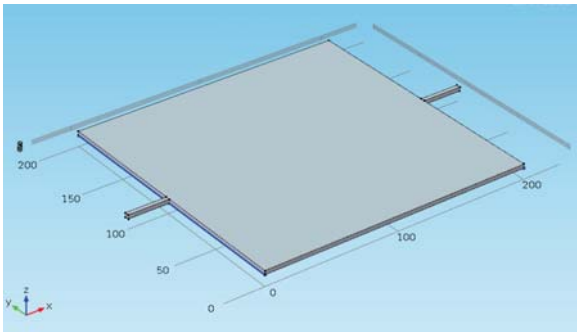

Figure 3.8: Tilting plate with two adjacent edges closed

Figure 3.9 compares the frequency responses between the analytical and COMSOL models. It shows a good agreement.

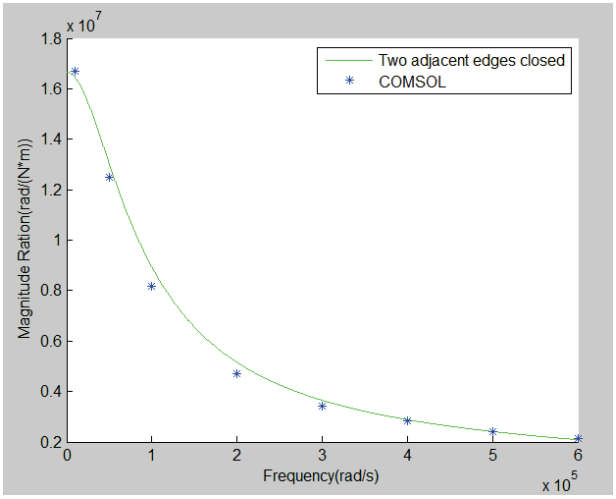

Figure 3.9: Comparison of simulated and analytical results

After confirming that this model with two adjacent edges works, the model for element 'A' in Figure 3.7 can be derived. The domain of the compressed area of element 'A' in Figure 3.7 is taken to be $a_1 \leq x \leq a_2$ and $b_1 \leq y \leq b_2$, corresponding to a rectangular plate of dimensions $a \times b$, where $a = a_2 - a_1$ and $b = b_2 - b_1$. The boundary conditions can be

expressed as $\frac{\partial P}{\partial x} = 0$ at $x = a_1$, and $\frac{\partial P}{\partial y} = 0$ at y $= b_1$ with venting P=0 along the other two edges of $x = a_2$ and $y = b_2$. According to these boundary conditions, the eigenfunctions become:

$$u_{mn}(x,y) = \sqrt{\frac{4}{ab}} \cos\frac{m\pi}{2a}(x - a_1)\cos\frac{n\pi}{2b}(y - b_1) \tag{3.21}$$

Where *m, n= {1, 3, 5…..}*. The associated eigenvalues are

$$k_{mn} = \frac{m^2\pi^2}{4a^2} + \frac{n^2\pi^2}{4b^2} \tag{3.22}$$

Following the approach described in Darling's paper, the normalized pressure distribution for this kind of plate can be derived as

$$P(x,y,t) = \sum_{\substack{m=odd \\ n=odd}} \frac{32(-1)^{\frac{n-1}{2}}}{\pi^3 m^2 na} \frac{-j\omega H' e^{j\omega t}}{j\omega + k^2_{mn}/a^2} \left(\pi m a_2 (-1)^{\frac{m-1}{2}} - 2a\right) \cos\frac{m\pi}{2a}(x - a_1)\cos\frac{n\pi}{2b}(y - b_1) \tag{3.23}$$

The restoring torque on the plate can be computed as:

$$\tau(t) = P_a \int_{a_1}^{a_2}\int_{b_1}^{b_2} xP(x,y,t)dxdy$$

$$= \sum_{\substack{m=odd \\ n=odd}} P_a \frac{-j\omega H' e^{j\omega t}}{j\omega + k^2_{mn}/a^2} \frac{128ab}{a\pi^6 m^4 n^2} \left(\pi m a_2 (-1)^{\frac{m-1}{2}} - 2a\right)^2 \tag{3.24}$$

The real part value is the torsional spring stiffness *(k)* of air, the imaginary part value is the torsional damping (b) of air. The stiffness of air underneath tilting plate is the real component of the reaction force divided by the tip displacement.

$$k_{spring} = \tau(t)_{Re}/H'$$

$$= Re\left[\sum_{\substack{m=odd \\ n=odd}} P_a \frac{-j\omega e^{j\omega t}}{j\omega + k^2_{mn}/a^2} \frac{128ab}{a\pi^6 m^4 n^2} \left(\pi m a_2 (-1)^{\frac{m-1}{2}} - 2a\right)^2\right] \tag{3.25}$$

Similarly, the damping coefficient of air underneath tilting plate can be determined from the imaginary component of the reaction force divided by the tip velocity:

$$b_{damping} = \tau(t)_{Im}/v$$

$$= Im\left[\sum_{\substack{m=odd \\ n=odd}} P_a \frac{-je^{j\omega t}}{j\omega + k^2_{mn}/a^2} \frac{128ab}{a\pi^6 m^4 n^2} \left(\pi m a_2 (-1)^{\frac{m-1}{2}} - 2a\right)^2\right] \tag{3.26}$$

3.1.2.2 Element 'B' with two opposite edges closed along the y axis

The domain of the compressed area of element 'B' in Figure 3.7 has two opposite edges closed along the *y* axis. The derivation of the analytical equation for element 'B' begins with the equation for the regular tilting plate. Following the same procedure as for element

'A', the two opposite edges closed are expressed as $\frac{\partial P}{\partial y} = 0$ at $y = -\frac{b}{2}$, $y = \frac{b}{2}$, with ideal venting P=0 along the remaining two edges of $x = \frac{a}{2}$, $x = -\frac{a}{2}$. The eigenfunctions are:

$$u_{mn}(x,y) = \sqrt{\frac{2}{ab}} \cos sin \frac{m\pi}{a} x \tag{3.27}$$

Where *cos* is used for *m*= odd; *sin* is used for *m*= even. The corresponding eigenvalues are

$$k_m = \frac{m^2\pi^2}{a^2} \tag{3.28}$$

The restoring torque on the plate can be computed as:

$$\tau(t) = \sum_{m=even} Pa \frac{-jwH'e^{jwt}}{jw+k^2{}_m/a^2} \frac{4a^2b}{\pi^2m^2} \tag{3.29}$$

The stiffness of air underneath the tilting plate is the spring component of the reaction force divided by the tip displacement.

$$k_{spring} = \tau(t)/H'$$

$$= Re[\sum_{m=even} Pa \frac{-j\omega e^{j\omega t}}{jw+k^2{}_m/a^2} \frac{4a^2b}{\pi^2m^2}] \tag{3.30}$$

Similarly, the damping coefficient of air underneath the tilting plate can be determined from the damping component of the reaction force divided by the tip velocity:

$$b_{damping} = \tau(t)/v$$

$$= Im[\sum_{m=even} Pa \frac{-je^{j\omega t}}{j\omega+k^2{}_m/a^2} \frac{4a^2b}{\pi^2m^2}] \tag{3.31}$$

For the COMSOL model, a "wall" is created at these edges which will block any air flow.

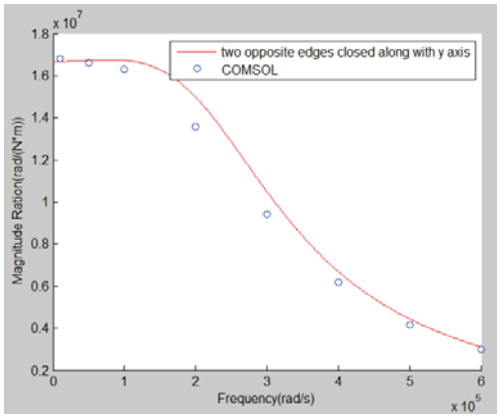

Figure 3.10: Compare the simulate result and analytical result

Figure 3.10 shows the simulated result and analytical result match well, we can start to integral the analytical model of element B shown in Figure 3.7.

The domain of the compressed area of element 'B' in Figure 3.7 is taken to be $a_1 \leq x \leq a_2$ and $b_1 \leq y \leq b_2$, corresponding to a rectangular plate of dimensions $a \times b$, where $a = a_2 - a_1$ and $b = b_2 - b_1$. The boundary conditions can be expressed as $\frac{\partial P}{\partial y} = 0$ at $y = b_1$ and $y = b_2$. With venting $P=0$ along the other two edges of $x = a_1$ and $x = a_2$. According to these boundary conditions, the eigenfunctions become:

$$u_{mn}(x,y) = \sqrt{\frac{2}{ab}} \begin{matrix} \cos \\ sin \end{matrix} \frac{m\pi}{a}(x - a') \tag{3.32}$$

Where *cos* is used for *m*= odd; *sin* is used for *m*= even. The corresponding eigenvalues are

$$k_m = \frac{m^2\pi^2}{a^2} \tag{3.33}$$

The normalized pressure distribution for this kind of plate can be derived as

$$P(x,y,t) = \frac{4}{L}\left[\sum_{m=odd} \frac{-j\omega H' e^{j\omega t}}{j\omega + k^2{}_n/a^2} \times (a_1 + a_2)(-1)^{\frac{n-1}{2}} cos\frac{m\pi}{a}(x - a') + \sum_{m=even} \frac{-j\omega H' e^{j\omega t}}{j\omega + k^2{}_n/a^2} \times (a_1 - a_2)(-1)^{\frac{n}{2}} sin\frac{m\pi}{a}(x - a')\right] \tag{3.34}$$

The restoring torque on the plate can be computed as:

$$\tau(t) = P_a \int_{a_1}^{a_2} \int_{b_1}^{b_2} xP(x,y,t)dxdy$$

$$= \sum_{n=odd} \frac{-j\omega H' e^{j\omega t}}{j\omega + k^2{}_n/a^2} \times \frac{4\text{ab}}{L\pi^2 n^2}(a_1 + a_2)^2 + \sum_{n=even} \frac{-j\omega H' e^{j\omega t}}{j\omega + k^2{}_n/a^2} \times \frac{4\text{ab}}{L\pi^2 n^2}(a_1 - a_2)^2 \tag{3.35}$$

The real part value is the torsional spring stiffness (*k*) of air, the imaginary part value is the torsional damping (*b*) of air. The stiffness of air underneath tilting plate is the real component of the reaction force divided by the tip displacement.

$$k_{spring} = \tau(t)/H'$$

$$= Re\left[\sum_{n=odd} \frac{-j\omega e^{j\omega t}}{j\omega + k^2{}_n/a^2} \times \frac{4\text{ab}}{L\pi^2 n^2}(a_1 + a_2)^2 + \sum_{n=even} \frac{-j\omega e^{j\omega t}}{j\omega + k^2{}_n/a^2} \times \frac{4\text{ab}}{L\pi^2 n^2}(a_1 - a_2)^2\right] \tag{3.36}$$

Similarly, the damping coefficient of air underneath tilting plate can be determined from the imaging component of the reaction force divided by the tip velocity:

$$b_{damping} = \tau(t)/v$$

$$= Im[\sum_{n=odd} \frac{-je^{j\omega t}}{j\omega + k^2{}_n/a^2} \times \frac{4\text{ab}}{L\pi^2 n^2}(a_1 + a_2)^2 + \sum_{n=even} \frac{-je^{j\omega t}}{j\omega + k^2{}_n/a^2} \times \frac{4\text{ab}}{L\pi^2 n^2}(a_1 - a_2)^2] \quad (3.37)$$

3.1.2.3 Element 'C' with two opposite edges closed along the x axis

The domain of the compressed area of element 'C' in Figure 3.7 has two opposite edges closed along the *y* axis. The two opposite edges closed are expressed as $\frac{\partial P}{\partial x} = 0$ at $x = -\frac{a}{2}$, $x = \frac{a}{2}$, with ideal venting P=0 along the remaining two edges of $y = \frac{b}{2}$, $y = -\frac{b}{2}$, the eigenfunctions are:

$$u_{mn}(x, y) = \sqrt{\frac{2}{ab}} \cos \sin \frac{n\pi}{b}(y) \quad (3.38)$$

Where *cos* is used *n* is equal to odd, *sin* is used for *n* is equal to even. The corresponding eigenvalues are

$$k_{mn} = \frac{n^2\pi^2}{b^2} \quad (3.39)$$

The normalized pressure distribution for this kind of plate can be derived as

$$P(x, y, t) = \sum_{n=odd} \frac{8x}{\pi nL} \times (-1)^{\frac{n-1}{2}} \frac{-j\omega H' e^{j\omega t}}{j\omega + k^2{}_{mn}/a^2} \times \cos \frac{n\pi}{b}(y) \quad (3.40)$$

The restoring torque on the plate can be computed as:

$$\tau(t) = \sum_{n=odd} Pa \frac{-j\omega H' e^{j\omega t}}{j\omega + k^2{}_{mn}/a^2} * \frac{4\text{a}^3 * \text{b}}{3\pi^2 * n^2 L} \quad (3.41)$$

The stiffness of air underneath tilting plate is the spring component of the reaction force divided by the tip displacement.

$$k_{spring} = \tau(t)/H'$$

$$= Re[\sum_{n=odd} Pa \frac{-j\omega e^{j\omega t}}{j\omega + k^2{}_{mn}/a^2} * \frac{4\text{a}^3 * \text{b}}{3\pi^2 * n^2 L}] \quad (3.42)$$

Similarly, the damping coefficient of air underneath tilting plate can be determined from the damping component of the reaction force divided by the tip velocity:

$$b_{damping} = \tau(t)/v$$

$$= Im[\sum_{n=odd} Pa \frac{-je^{j\omega t}}{j\omega + k^2_{mn}/a^2} * \frac{4a^3 * b}{3\pi^2 * n^2 L}] \quad (3.43)$$

Walls are created in COMSOL to match the boundary conditions.

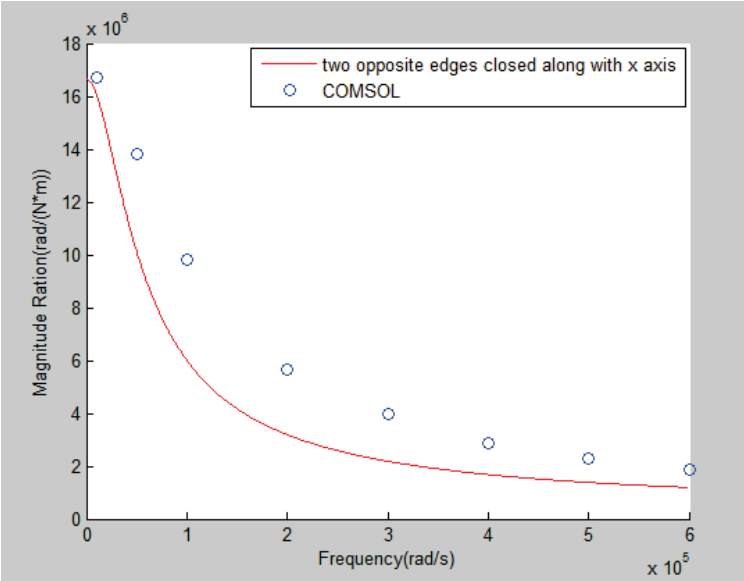

Figure 3.11: Comparison of the simulated result and analytical result

Figure 3.11 shows the simulated result and analytical result match well, we can start to integral the analytical model of element B shown in Figure 3.7.

The domain of the volume is taken to be $a_1 \leq x \leq a_2$ and $b_1 \leq y \leq b_2$, corresponding to a rectangular plate of dimensions $a \times b$, where $a = a_2 - a_1$ and $b = b_2 - b_1$. Plate 'B' has two opposite edges closed along the x axis, the boundary conditions can be expressed as $\frac{\partial P}{\partial x} = 0$ at $x = a_1$, and $x = a_2$. With venting P=0 along the other two edges of $y = b_1$ and $y = b_2$. According to these boundary conditions, the eigenfunctions become:

$$u_{mn}(x, y) = \sqrt{\frac{2}{ab}} \cos \sin \frac{n\pi}{b}(y - b') \quad (3.44)$$

Where *cos* is used for *n* is equal to odd, *sin* is used for *n* is equal to even. Here, $b' = \frac{(b_2 + b_1)}{2}$. The associated eigenvalues are

$$k_{mn} = \frac{n^2\pi^2}{b^2} \quad (3.45)$$

The normalized pressure distribution for this kind of plate can be derived as

$$P(x,y,t) = \sum_{n=odd} \frac{8x(-1)^{\frac{n-1}{2}}}{\pi nL} \frac{-j\omega H' e^{j\omega t}}{j\omega + k^2{}_{mn}/a^2} * \cos\frac{m\pi}{b}(y - b') \tag{3.46}$$

The restoring torque on the plate can be computed as:

$$\tau(t) = P_a \int_{a_1}^{a_2} \int_{b_1}^{b_2} xP(x,y,t)dxdy$$

$$= \sum_{n=odd} Pa \frac{-j\omega H' e^{j\omega t}}{j\omega + k^2{}_{mn}/a^2} * \frac{16\mathrm{b}(a_2{}^3 - a_1{}^3)}{3L*\pi^2*n^2} \tag{3.47}$$

The stiffness of air underneath tilting plate is the spring component of the reaction force divided by the tip displacement.

$$k_{spring} = \tau(t)/H'$$

$$= Re[\sum_{n=odd} P_a \frac{-j\omega e^{j\omega t}}{j\omega + k^2{}_{mn}/a^2} * \frac{16\mathrm{b}(a_2{}^3 - a_1{}^3)}{3L*\pi^2*n^2}] \tag{3.48}$$

Similarly, the damping coefficient of air underneath tilting plate can be determined from the damping component of the reaction force divided by the tip velocity:

$$b_{damping} = \tau(t)/v$$

$$= Im[\sum_{n=odd} P_a \frac{-je^{j\omega t}}{j\omega + k^2{}_{mn}/a^2} * \frac{16\mathrm{b}(a_2{}^3 - a_1{}^3)}{3L*\pi^2*n^2}] \tag{3.49}$$

3.1.3 Comparison of the frequency responses of analytical and COMSOL models

After building the analytical equations of all three elements, the analytical model of tilting plate with a hole in the center can be formed. According to the restoring torque of the three elements shown above, the k_{air} and b_{air} are all corresponding to the maximum z displacement occurring at $x = \pm \mathrm{a}/2$, (H'). So it is reasonable to get the $k_{total,air}$ and $b_{total,air}$ by adding k_{air} and b_{air} of the elements together. As shown in Figure 3.7, the tilting plate has 8 elements which are combined by 4 of element 'A', 2 of element 'B' and 2 of element 'C'. The total air stiffness and air damping can be expressed as:

$$k_{total,air} = 4k_a + 2k_b + 2k_c \tag{3.50}$$

$$b_{total,air} = 4b_a + 2b_b + 2b_c \tag{3.51}$$

The mass moment of inertia (I) can be calculated by:

$$I = \frac{1}{12} m_{big} a^2 - \frac{1}{12} m_{small} s^2 \tag{3.52}$$

Where m_{big} is the mass of the original plate, a is the length of the original plate. And m_{small} is the mass of the square hole plate, s is the length of the plate as a hole.

The transfer function is the same as for the regular tilting plate,

$$\frac{\theta(t)}{\tau(t)} = \sqrt{\frac{1}{\left((k_{flex}+k_{air,total}(\omega))-I\times\omega(t)^2\right)^2+\left(b_{air,total}(\omega)\times\omega(t)\right)^2}} \tag{3.53}$$

Where b is the damping coefficient of air, and k is the sum of stiffness of support beams and air.$k = k_{flex} + k_{air}$. The support beam torsional stiffness (k_{flex}) is 6e-8 *N-m/rad* in the analytical model.

Then, the analytical frequency response of the tilting plate can be calculated with MATLAB by using the parameters shown in Table 3.2.

Table 3. 2: Parameter used in both analytical and simulated tilting plate models

Pa	101000 Pa
$\mu_{effective}$	1.862×10^{-5} Pa.s
L	200 µm
W	200 µm
t	3 µm
ρ	2330 kg/m^3
m	2.796×10^{-10} kg
g_0	4 µm
k_{flex}	$6 \times 10^{-8} Nm/rads$
s (hole size)	50 µm × 50 µm

Simulated model in COMSOL MULTIPHYSICS

The procedure for creating a model that matches the analytical is:

1. Sketch a tilting plate in COMSOL MULTIPHYSICS using the same parameters as in analytical model.
2. The hole in the center is using Boolean Operations by subtracting the big square plate and small square plate (hole) so that this model is one element.
3. From the time response, collect each maximum displacement value of the free edge for different input frequencies. The simulated magnitude ratio is equal to the angle θ divided by the torque τ.

Figure 3.12 shows the mesh for the COMSOL model. The 'Free Tetrahedral' element is used. The element shape is triangle and it has three nodes. According to the test, mesh dimension of 'Coarse' is sufficient for the mesh optimization, and the elements at the corners of the hole are well connected. This model has 5200 elements; it will take 10-15 minutes to get one frequency response point.

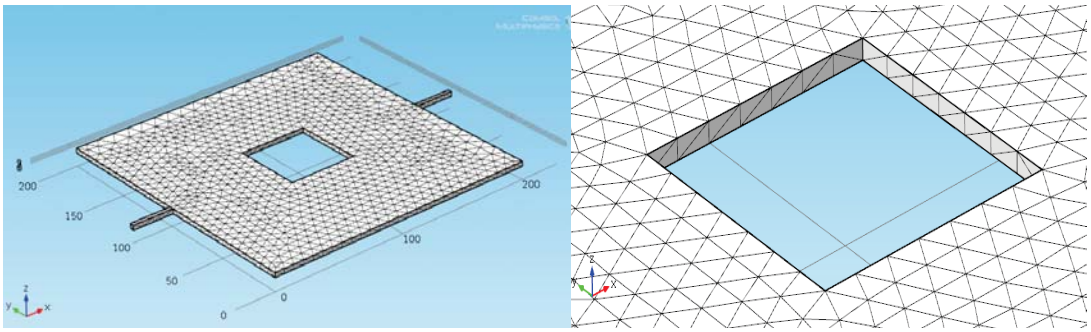

Figure 3.12: Mesh for the COMSOL model

Figure 3.13 shows the air damping pressure distribution in COMSOL of 200 μm × 200 μm tilting plate with a 50 μm × 50 μm hole in the center. The highest air damping pressure occurs at the edge between the two adjacent edges closed element and two opposite edges closed element. This is reasonable because no air crosses that edge.

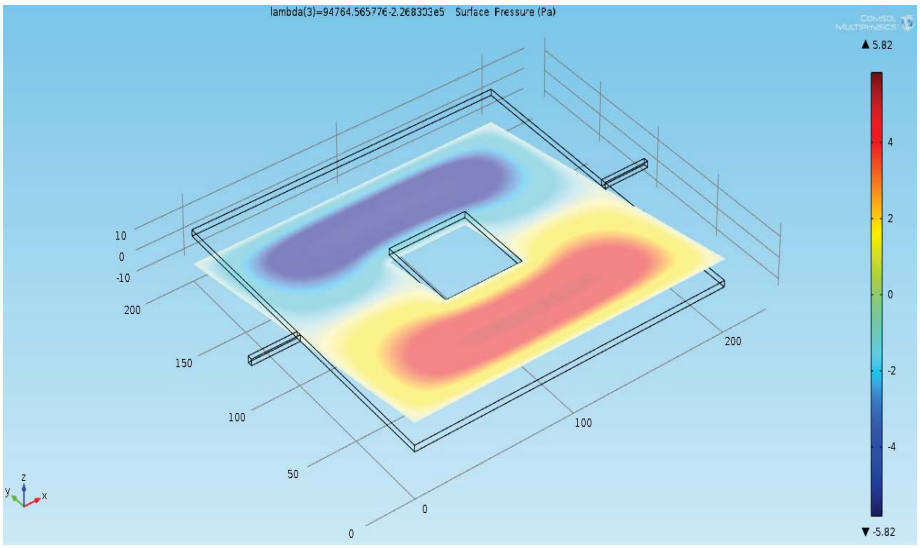

Figure 3.13: The air damping pressure distribution on the surface

Figure 3.14 shows the frequency response. This tilting plate is a 200(um) × 200(um) square plate with a 50(um) × 50(um) hole in the center. The results indicate that the analytical model matches the simulation very well. Three more models are built in order to identify the analytical model.

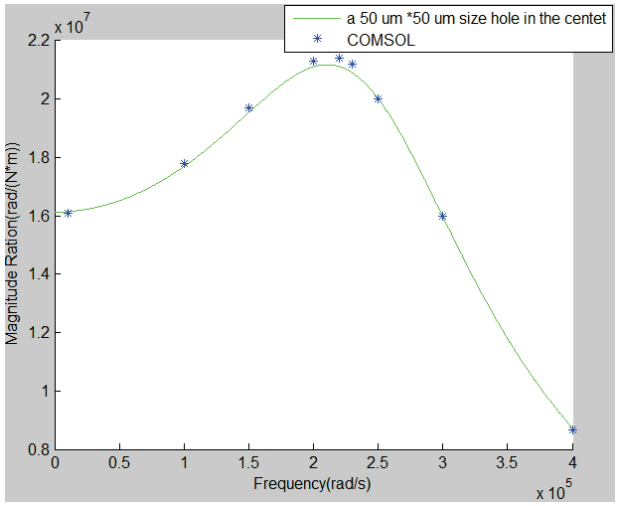

Figure 3.14: The 200(um) *200(um) tilting plate with a hole in the center

Figure 3.15 shows additional comparisons for different hole size tilting plates. The results indicate that the analytical model matches the simulation very well. The analytical frequency response can be produced in 1 minute, but each point of the simulation result needs at least 10 minutes or 90 minutes for the 9 points in Figure 3.13(a). So the analytical model is much more efficient. The air damping will influence the magnitude ratio; the magnitude ratio at the resonant frequency increases when the air damping decreases. Figure 3.15 shows that increasing the hole size reduces the air damping. On the other hand, a large hole reduces the plate area available for actuation, sensing and also absorbing the chemical materials. This analytical model can be used to do design optimization.

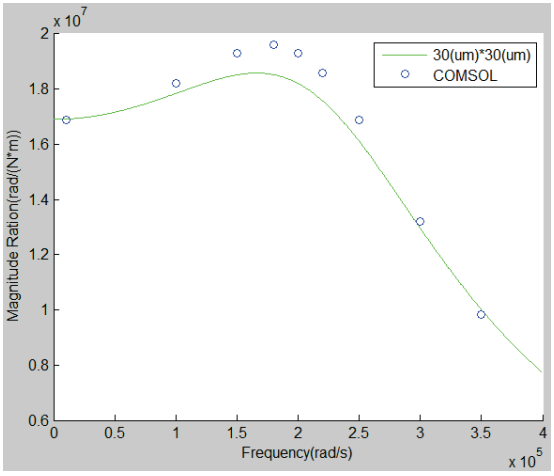

(a)

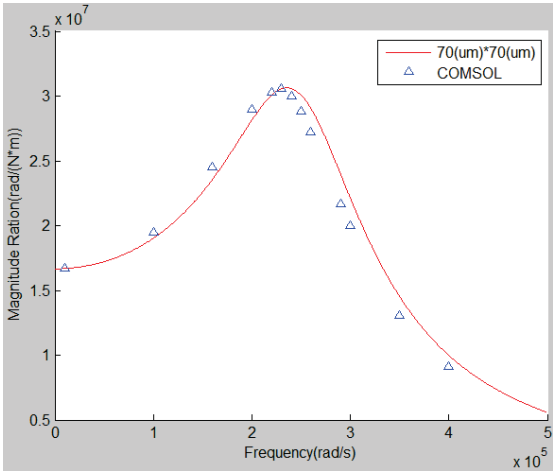

(b)

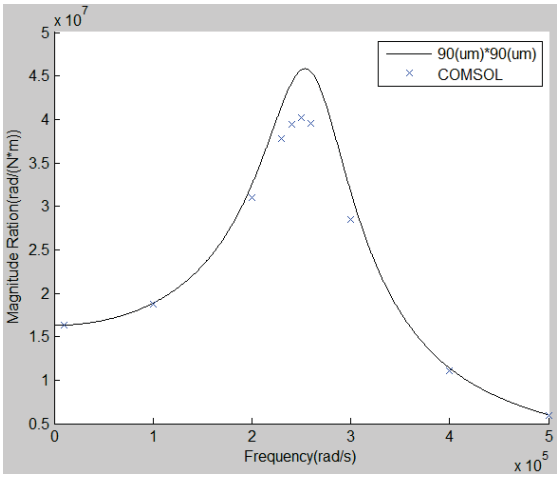

(c)

Figure 3.15: The 200(um) *200(um) tilting plate with a different hole size in the center

3.2 Square Tilting plate about its diagonal

This section derives an analytical squeeze film damping model of a tilting plate about its diagonal according to the Green's function approach used in previous section. A rigid rectangular plate connected by two leg beams at the corner and it's consider as a fixed-free torsional beam. The gap between the plate and the substrate is uniform held as a constant if the plate is not oscillating.

3.2.1 Analytical model of square tilting plate without holes

This section builds an analytic damping force model of a square tilting plate about its diagonal using the Green's function. The domain of the tilting plate is $-\frac{a}{2} < x < \frac{a}{2}$ and $-\frac{a}{2} < y < \frac{a}{2}$, corresponding to a rectangular plate with length a and width a. The four edges are assumed to have ideal venting, and the plate tilts about its diagonal $y = -x$. The plate can be represented with a model as shown in Figure 3.16.

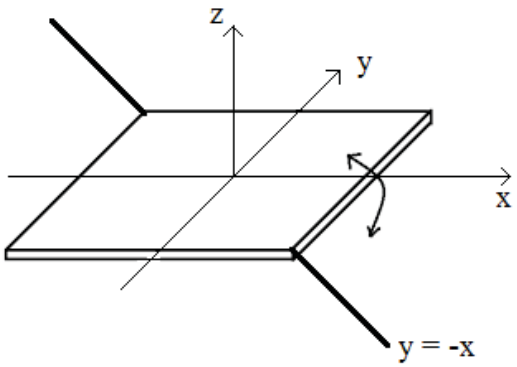

Figure 3.16: The tilting plate about its diagonal

For this plate, the normalized displacement is approximated as:

$$H(x, y, t) = H' \frac{x+y}{a} e^{j\omega t} \tag{3.54}$$

Where $H'$is the normalized magnitude of displacement in *z* direction, $H' = \frac{x+y}{h_0}$, and h_0 is the displacement occurs at the tip of $(\frac{a}{2}, \frac{a}{2})$ and $(-\frac{a}{2}, -\frac{a}{2})$. The maximum angle of rotation can be described as:

$$\theta_{max} = tan^{-1}\sqrt{2}h_o H'/a \tag{3.55}$$

Because the boundary condition is ideal venting on four edges in this situation, the eigenfunctions u_{mn} and eigenvalues k_{mn} calculated by two-dimensional scalar Helmholtz equation can described as:

$$u_{mn}(x,y) = \sqrt{\frac{4}{ab}} \begin{matrix}\cos \\ sin\end{matrix} \frac{m\pi}{a}(x) \begin{matrix}\cos \\ sin\end{matrix} \frac{n\pi}{b}(y) \tag{3.56}$$

Where cos is used for *m, n = {1, 3, 5….}* and sin is used for *m, n = {2, 4, 6….}*. The corresponding eigenvalues are:

$$k_{mn} = \frac{m^2\pi^2}{a^2} + \frac{n^2\pi^2}{b^2} \tag{3.57}$$

The normalized pressure can be calculated by the integral equation shown in Darling's paper:

$$P(x,y,t) = \sum_{\substack{m=even \\ n=odd}} \frac{8(-1)^{m/2-1}(-1)^{(n-1)/2}}{\pi^2 mn} \frac{-j\omega H' e^{j\omega t}}{j\omega + k^2{}_{mn}/a^2} sin\frac{m\pi x}{a} cos\frac{n\pi y}{b} + \sum_{\substack{m=odd \\ n=even}} \frac{8(-1)^{(m-1)/2}(-1)^{n/2-1}}{\pi^2 mn} \frac{-j\omega H' e^{j\omega t}}{j\omega + k^2{}_{mn}/a^2} cos\frac{m\pi x}{a} sin\frac{n\pi y}{b} \tag{3.58}$$

Where *m = (2, 4, 6…)* and *n = (1, 3, 5…)*. The torque is calculated by force times the distance, so the normalized restoring torque can be described as:

$$\begin{aligned}\tau(t) &= P_a \int_{-a/2}^{+a/2} \int_{-b/2}^{+b/2} \frac{x+y}{\sqrt{2}} P(x,y,t) dxdy \\ &= \sum_{\substack{m=even \\ n=odd}} \frac{32a^3 P_a}{\sqrt{2}\pi^4 m^2 n^2} \frac{-j\omega H' e^{j\omega t}}{j\omega + k^2{}_{mn}/a^2}\end{aligned} \tag{3.59}$$

P_a is the ambient pressure.

According to the Hooke's law,

$$\tau = Fd = k\theta \tag{3.60}$$

The rotational angle θ is calculated by the maximum displacement at the tip divided by half length of the diagonal, $\theta = \frac{V_{tip}}{\sqrt{2}a/2}$. The torque can then be rewritten as:

$$\begin{aligned}\frac{\tau(t)}{a^2 P_a} &= \sum_{\substack{m=even \\ n=odd}} \frac{32}{\pi^4 m^2 n^2} \frac{-j\omega e^{j\omega t}}{j\omega + k^2{}_{mn}/a^2} \frac{\sqrt{2}a}{2} H' \\ &= \sum_{\substack{m=even \\ n=odd}} \frac{32}{\pi^4 m^2 n^2} \frac{-j\omega e^{j\omega t}}{j\omega + k^2{}_{mn}/a^2} \frac{\sqrt{2}a}{2} \frac{V_{tip}}{h_0} \\ &= \sum_{\substack{m=even \\ n=odd}} \frac{32}{h_0 \pi^4 m^2 n^2} \frac{-j\omega e^{j\omega t}}{j\omega + k^2{}_{mn}/a^2} \left(\frac{\sqrt{2}a}{2}\right)^2 \frac{V_{tip}}{\frac{\sqrt{2}a}{2}} \\ &= \sum_{\substack{m=even \\ n=odd}} \frac{32}{h_0 \pi^4 m^2 n^2} \frac{-j\omega e^{j\omega t}}{j\omega + k^2{}_{mn}/a^2} \left(\frac{\sqrt{2}a}{2}\right)^2 \theta\end{aligned} \tag{3.61}$$

The normalized restoring torque function can be used to find stiffness and damping of air. The real part value is the spring component (k) of air, which is calculated by the reaction torque divided by the rotational angle (θ). The imaginary part value is the damping component (b) of air, which can be calculated by the reaction torque divided by the rotation angle velocity ($w\theta$):

$$k_{air} = Re(\sum_{\substack{m=even \\ n=odd}} \frac{32}{h_0\pi^4 m^2 n^2} \frac{-j\omega e^{j\omega t}}{j\omega + \frac{k^2 mn}{a^2}} \left(\frac{\sqrt{2}a}{2}\right)^2 a^2 P_a) \tag{3.62}$$

$$b_{air} = Im(\sum_{\substack{m=even \\ n=odd}} \frac{32}{h_0\pi^4 m^2 n^2} \frac{-je^{j\omega t}}{j\omega + \frac{k^2 mn}{a^2}} \left(\frac{\sqrt{2}a}{2}\right)^2 a^2 P_a) \tag{3.63}$$

According to the Newton's second law and the free body diagram, the equation of motion for a second order rotational system is:

$$I\ddot{\theta}(t) + b(\omega)\dot{\theta}(t) + k(\omega)\theta(t) = \tau(t) \tag{3.64}$$

Where b is the damping coefficient of air, and k is the sum of stiffness of material and air. $k = k_{flex} + k_{air}$. I is the mass moment of inertia, which can be calculated by:

$$I = \frac{1}{12}ma^2 \tag{3.65}$$

The magnitude ratio function can be expressed as:

$$\frac{\theta(t)}{\tau(t)} = \sqrt{\frac{1}{\left((k_{flex}+k_{air}(\omega))-I\times\omega(t)^2\right)^2 + (b_{air}(\omega)\times\omega(t))^2}} \tag{3.66}$$

Then, the analytical frequency response of the tilting plate can be calculated with MATLAB by using the parameters shown in Table 3.3.

Table 3. 3: Parameter used in both analytical and simulated tilting plate models

Pa	101000 Pa
$\mu_{effective}$	1.862× 10^{-5} $Pa.s$
L	200 μm
W	200 μm
t	3 μm
ρ	2330 kg/m^3
m	2.796× 10^{-10} kg
g_0	4 μm
k_{flex}	$2 \times 10^{-7} Nm/rads$

Simulated model in COMSOL MULTIPHYSICS

Figure 3.17 is showing the COMSOL model is created as before except that silicon beams (representing torsional springs) are connected at two diagonal corners of the plate.

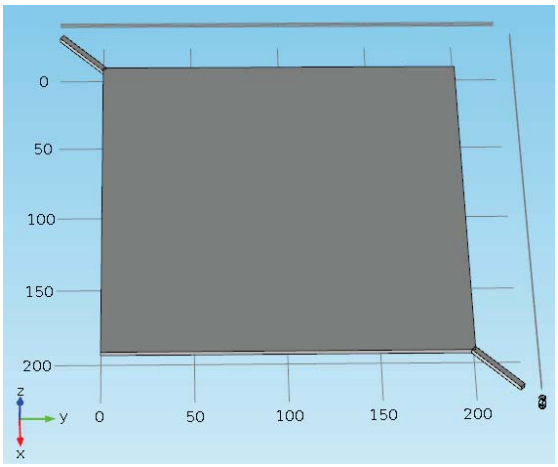

Figure 3.17: Tilting plate about its diagonal in COMSOL

Figure 3.18 compare the frequency responses of the analytical and COMSOL models. For this model, the analytical result are pretty close to the simulation results.

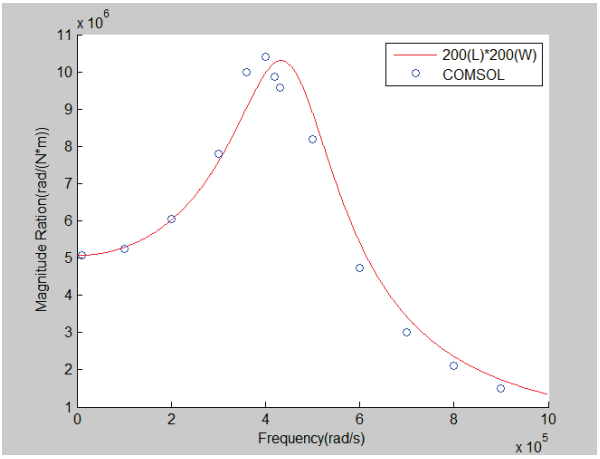

Figure 3.18: The frequency response of tilting plate about its diagonal

3.2.2 Tilting plate about the y axis with a hole in the center

Adding a hole in the center of tilting plate would reduce the air damping and increase the Q value. Different hole sizes are tested during the design process. The tilting plate is divided into eight kinds of rectangular plates with four different boundary conditions. As Figure 3.19 shows, Element 'A' has two adjacent edges closed, element 'B' has two adjacent edges closed, element 'C' has two opposite edges closed along the *x* axis, and element 'D' has two opposite edges closed along the *y* axis. The analytical equations of each element can be derived.

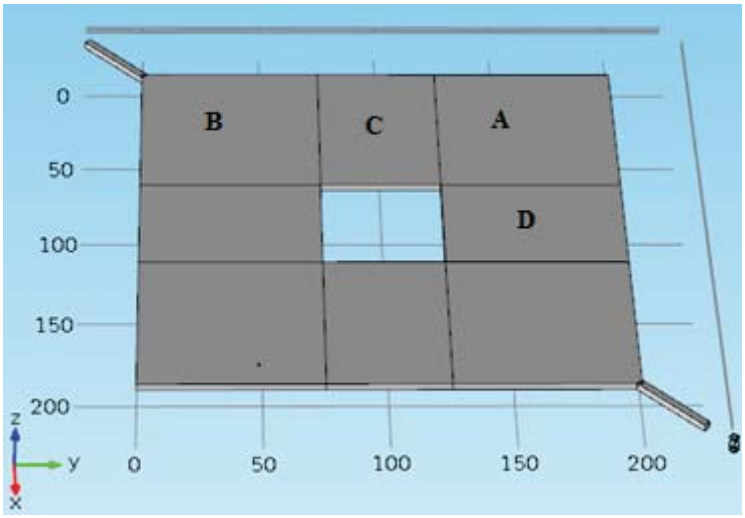

Figure 3.19: Tilting plate about its diagonal with a hole in the center

The square plate in Fig 3.19 has length "a" and it tilts about its diagonal. The maximum displacement in *z* direction occurs at the tip of $(\frac{a}{2}, \frac{a}{2})$ and $(-\frac{a}{2}, -\frac{a}{2})$. It can be described as:

$$H(x, y, t) = H' \frac{x+y}{a} e^{j\omega t} \tag{3.67}$$

Where H' is the normalized maximum displacement at the tip of $(\frac{a}{2}, \frac{a}{2})$ and $(-\frac{a}{2}, -\frac{a}{2})$.

Element A with two adjacent edges closed

The domain of the compressed area of element 'A' in Figure 3.19 is taken to be $a_1 \leq x \leq a_2$ and $b_1 \leq y \leq b_2$, corresponding to a rectangular plate of dimensions $a \times b$, where $a = a_2 - a_1$ and $b = b_2 - b_1$. Plate 'A' has two adjacent edges closed, the boundary conditions can be expressed as $\frac{\partial P}{\partial x} = 0$ at $x = a_1$, and $\frac{\partial P}{\partial y} = 0$ at $y = b_1$. With venting P=0 along the other two

edges of $x= a_2$ and $y=b_2$. According to these boundary conditions, the eigenfunctions become:

$$u_{mn}(x,y) = \sqrt{\frac{4}{ab}}\cos\frac{m\pi}{2a}(x-a_1) * \cos\frac{n\pi}{2b}(y-b_1) \tag{3.68}$$

Where *m, n= {1, 3, 5…..}*. The associated eigenvalues are

$$k_{mn} = \frac{m^2\pi^2}{4a^2} + \frac{n^2\pi^2}{4b^2} \tag{3.69}$$

Following the approach described in Darling's paper, the normalized pressure distribution for this kind of plate can be derived as

$$P(x,y,t) = \sum_{\substack{m=odd\\n=odd}} \frac{16}{\pi^3 m^2 n^2 L}\left[n\left(m\pi(a_2+b_2)\times(-1)^{\frac{m-1}{2}} - 2a\right)\times(-1)^{\frac{n-1}{2}} - 2mb(-1)^{\frac{m-1}{2}}\right]\frac{-j\omega H' e^{j\omega t}}{j\omega + k^2_{mn}/a^2}\times\cos\frac{m\pi}{2a}(x-a_1)\times\cos\frac{n\pi}{2b}(y-b_1) \tag{3.70}$$

The restoring torque on the plate can be computed as:

$$\tau(t) = P_a\int_{a_1}^{a_2}\int_{b_1}^{b_2}\frac{(x+y)}{\sqrt{2}}P(x,y,t)dxdy$$

$$= \sum_{\substack{m=odd\\n=odd}} P_a\frac{-j\omega H' e^{j\omega t}}{j\omega + k^2_{mn}/a^2}\times\frac{64\text{ab}}{\sqrt{2}L*\pi^6*m^4*n^4}\times\left(n\left(m\pi(a_2+b_2)\times(-1)^{\frac{m-1}{2}} - 2a\right)\times(-1)^{\frac{n-1}{2}} - 2mb(-1)^{\frac{m-1}{2}}\right)^2 \tag{3.71}$$

The real part value is the spring stiffness (*k*) of air, the imaginary part value is the damping (*b*) of air. The stiffness of air underneath tilting plate is the spring component of the reaction force divided by the tip displacement.

$$k_{spring} = \tau(t)/H'$$

$$= Re[\sum_{\substack{m=odd\\n=odd}} P_a\frac{-j\omega e^{j\omega t}}{j\omega + k^2_{mn}/a^2} * \frac{64\text{ab}}{\sqrt{2}L*\pi^6*m^4*n^4}\times\left(n\left(m\pi(a_2+b_2)\times(-1)^{\frac{m-1}{2}} - 2a\right)\times(-1)^{\frac{n-1}{2}} - 2mb(-1)^{\frac{m-1}{2}}\right)^2] \tag{3.72}$$

Similarly, the damping coefficient of air underneath tilting plate can be determined from the damping component of the reaction force divided by the tip velocity:

$$b_{damping} = \tau(t)/v$$

$$= Im[\sum_{\substack{m=odd\\n=odd}} P_a\frac{-je^{j\omega t}}{j\omega + k^2_{mn}/a^2}\times\frac{64\text{ab}}{\sqrt{2}L*\pi^6*m^4*n^4} * \left(n\left(m\pi(a_2+b_2)\times(-1)^{\frac{m-1}{2}} - 2a\right)\times(-1)^{\frac{n-1}{2}} - 2mb(-1)^{\frac{m-1}{2}}\right)^2] \tag{3.73}$$

Element B with two adjacent edges closed

The domain of the compressed area of element 'B' in Figure 3.9 is taken to be $a_1 \leq x \leq a_2$ and $b_1 \leq y \leq b_2$, corresponding to a rectangular plate of dimensions $a \times b$, where $a = a_2$-

$a_1$and $b = b_2$-b_1. Plate A has two adjacent edges closed, the boundary conditions can be expressed as $\frac{\partial P}{\partial x} = 0$ at $x = a_2$, and $\frac{\partial P}{\partial y} = 0$ at $y = b_1$. With venting P=0 along the other two edges of $x = a_1$ and $y = b_2$. According to these boundary conditions, the eigenfunctions become:

$$u_{mn}(x,y) = \sqrt{\frac{4}{ab}}\cos\frac{m\pi}{2a}(a_2 - x) * \cos\frac{n\pi}{2b}(y - b_1) \tag{3.74}$$

Where $m, n = \{1, 3, 5\ldots..\}$. The associated eigenvalues are

$$k_{mn} = \frac{m^2\pi^2}{4a^2} + \frac{n^2\pi^2}{4b^2} \tag{3.75}$$

The normalized pressure distribution for this kind of plate can be derived as

$$P(x,y,t) = \sum_{\substack{m=odd \\ n=odd}} \frac{16}{\pi^3 m^2 n^2 L}\left[n\left(m\pi(a_1+b_2)\times(-1)^{\frac{m-1}{2}} + 2a\right)\times(-1)^{\frac{n-1}{2}} - 2mb(-1)^{\frac{m-1}{2}}\right]\frac{-j\omega H' e^{j\omega t}}{j\omega + k^2_{mn}/a^2}\times\cos\frac{m\pi}{2a}(a_2 - x)\times\cos\frac{n\pi}{2b}(y - b_1) \tag{3.76}$$

The restoring torque on the plate is:

$$\tau(t) = P_a\int_{a_1}^{a_2}\int_{b_1}^{b_2}\frac{(x+y)}{\sqrt{2}}P(x,y,t)dxdy$$

$$= \sum_{\substack{m=odd \\ n=odd}} P_a\frac{-j\omega H' e^{j\omega t}}{j\omega + k^2_{mn}/a^2}\times\frac{64\text{ab}}{\sqrt{2}L*\pi^6*m^4*n^4}\times\left(n\left(m\pi(a_1+b_2)\times(-1)^{\frac{m-1}{2}} + 2a\right)\times(-1)^{\frac{n-1}{2}} - 2mb(-1)^{\frac{m-1}{2}}\right)^2 \tag{3.77}$$

The real part value is the spring stiffness (k) of air, the imaginary part value is the damping (b) of air. The stiffness of air underneath tilting plate is the spring component of the reaction force divided by the tip displacement.

$$k_{spring} = \tau(t)/H'$$

$$= Re\left[\sum_{\substack{m=odd \\ n=odd}} P_a\frac{-j\omega e^{j\omega t}}{j\omega + k^2_{mn}/a^2} * \frac{64\text{ab}}{\sqrt{2}L*\pi^6*m^4*n^4}\times\left(n\left(m\pi(a_1+b_2)\times(-1)^{\frac{m-1}{2}} + 2a\right)\times(-1)^{\frac{n-1}{2}} - 2mb(-1)^{\frac{m-1}{2}}\right)^2\right] \tag{3.78}$$

Similarly, the damping coefficient of air underneath tilting plate can be determined from the damping component of the reaction force divided by the tip velocity:

$$b_{damping} = \tau(t)/v$$

$$= Im\left[\sum_{\substack{m=odd \\ n=odd}} P_a\frac{-je^{j\omega t}}{j\omega + k^2_{mn}/a^2}\times\frac{64\text{ab}}{\sqrt{2}L*\pi^6*m^4*n^4} * \left(n\left(m\pi(a_1+b_2)\times(-1)^{\frac{m-1}{2}} + 2a\right)\times(-1)^{\frac{n-1}{2}} - 2mb(-1)^{\frac{m-1}{2}}\right)^2\right] \tag{3.79}$$

Element ‘C’ with two opposite edges closed along the x axis

The domain of the volume is taken to be $a_1 \leq x \leq a_2$ and $b_1 \leq y \leq b_2$, corresponding to a rectangular plate of dimensions $a \times b$, where $a = a_2 - a_1$ and $b = b_2 - b_1$. Plate ‘C’ has two opposite edges closed along the x axis, the boundary conditions can be expressed as $\frac{\partial P}{\partial x} = 0$ at $x = a_1$, and $x = a_2$. With venting P=0 along the other two edges of y= b_1 and y=b_2. According to these boundary conditions, the eigenfunctions become:

$$u_{mn}(x,y) = \sqrt{\frac{2}{ab}} \cos_{sin} \frac{n\pi}{b}(y - b') \tag{3.80}$$

Where *cos* is used for n is equal to odd, *sin* is used for n is equal to even. Here, $b' = \frac{(b_2 + b_1)}{2}$. The associated eigenvalues are

$$k_{mn} = \frac{n^2\pi^2}{b^2} \tag{3.81}$$

The normalized pressure distribution for this kind of plate can be derived as

$$P(x,y,t) = \sum_{n=even} \frac{-2b}{\pi nL} \times (-1)^{\frac{n}{2}} \times \frac{-j\omega H' e^{j\omega t}}{j\omega + k^2{}_{mn}/a^2} \times \sin\frac{n\pi}{b}(y - b') + \sum_{n=odd} \frac{2(2x + b_1 + b_2)}{\pi nL} \times (-1)^{\frac{n-1}{2}} \times \frac{-j\omega H' e^{j\omega t}}{j\omega + k^2{}_{mn}/a^2} \times \cos\frac{n\pi}{b}(y - b') \tag{3.82}$$

The restoring torque on the plate can be computed as:

$$\tau(t) = P_a \int_{a_1}^{a_2} \int_{b_1}^{b_2} \frac{(x+y)}{\sqrt{2}} P(x,y,t)\,dx\,dy$$

$$= \sum_{n=even} P_a \frac{-j\omega H' e^{j\omega t}}{j\omega + k^2{}_{mn}/a^2} \times \frac{\sqrt{2}\mathrm{b}^3\mathrm{a}}{L * \pi^2 * n^2} + \sum_{n=odd} Pa \frac{-jwH' e^{jwt}}{jw + k^2{}_{mn}/a^2} \times \frac{\sqrt{2}\mathrm{b} \times \left[(2a_2 + b_2 + b_1)^3 - (2a_1 + b_2 + b_1)^3\right]}{6 * L * \pi^2 * n^2} \tag{3.83}$$

The real part value is the spring stiffness (k) of air, the imaginary part value is the damping (b) of air. The stiffness of air underneath tilting plate is the spring component of the reaction force divided by the tip displacement.

$$k_{spring} = \tau(t)/H'$$

$$= Re\left[\sum_{n=even} P_a \frac{-j\omega H' e^{j\omega t}}{j\omega + k^2{}_{mn}/a^2} \times \frac{\sqrt{2}\mathrm{b}^3\mathrm{a}}{L * \pi^2 * n^2} + \sum_{n=odd} P_a \frac{-jwH' e^{jwt}}{jw + k^2{}_{mn}/a^2} \times \frac{\sqrt{2}\mathrm{b} \times \left[(2a_2 + b_2 + b_1)^3 - (2a_1 + b_2 + b_1)^3\right]}{6 * L * \pi^2 * n^2}\right] \tag{3.84}$$

Similarly, the damping coefficient of air underneath tilting plate can be determined from the damping component of the reaction force divided by the tip velocity:

$$b_{damping} = \tau(t)/v$$

$$= Im\left[\sum_{n=even} P_a \frac{-je^{j\omega t}}{j\omega + k^2{}_{mn}/a^2} \times \frac{\sqrt{2}\mathrm{b}^3\mathrm{a}}{L * \pi^2 * n^2} + \sum_{n=odd} P_a \frac{-je^{jwt}}{jw + k^2{}_{mn}/a^2} \times \frac{\sqrt{2}\mathrm{b} \times \left[(2a_2 + b_2 + b_1)^3 - (2a_1 + b_2 + b_1)^3\right]}{6 * L * \pi^2 * n^2}\right] \tag{3.85}$$

Element ‘D’ with two opposite edges closed along the y axis

The domain of the compressed area of element ‘D’ in Figure 3.19 is taken to be $a_1 \leq x \leq a_2$ and $b_1 \leq y \leq b_2$, corresponding to a rectangular plate of dimensions a × b, where a = a_2-a_1 and b = b_2-b_1. Plate ‘D’ has two opposite edges closed along the y axis, the boundary conditions can be expressed as $\frac{\partial P}{\partial y} = 0$ at $y = b_1$ and $y = b_2$. With venting P=0 along the other two edges of $x = a_1$ and $x = a_2$. According to these boundary conditions, the eigenfunctions become:

$$u_{mn}(x,y) = \sqrt{\frac{2}{ab}} \begin{matrix} \cos \\ sin \end{matrix} \frac{m\pi}{a}(x - a') \tag{3.86}$$

Where *cos* is used for *m*= odd; *sin* is used for *m*= even. The corresponding eigenvalues are

$$k_m = \frac{m^2\pi^2}{a^2} \tag{3.87}$$

Following the approach described in Darling’s paper, the normalized pressure distribution for this kind of plate can be derived as

$$P(x,y,t) = \sum_{n=even} \frac{-2a}{\pi nL} \times (-1)^{\frac{n}{2}} \times \frac{-j\omega H' e^{j\omega t}}{j\omega + k^2{}_{mn}/a^2} \times \sin\frac{n\pi}{a}(x - a') + \sum_{n=odd} \frac{2(2y + a_1 + a_2)}{\pi nL} \times (-1)^{\frac{n-1}{2}} \times \frac{-j\omega H' e^{j\omega t}}{j\omega + k^2{}_{mn}/a^2} \times \cos\frac{n\pi}{a}(x - a') \tag{3.88}$$

As the same integral way showed in Darling’s paper, the restoring torque on the plate can be computed as:

$$\begin{aligned} \tau(t) &= P_a \int_{a_1}^{a_2} \int_{b_1}^{b_2} \frac{(x+y)}{\sqrt{2}} P(x,y,t)\,dx\,dy \\ &= \sum_{n=even} P_a \frac{-j\omega H' e^{j\omega t}}{j\omega + k^2{}_{mn}/a^2} \times \frac{\sqrt{2}\mathrm{a}^3\mathrm{b}}{L*\pi^2*n^2} + \sum_{n=odd} P_a \frac{-j\omega H' e^{j\omega t}}{j\omega + k^2{}_{mn}/a^2} \times \frac{\sqrt{2}\mathrm{a} \times \left[(2b_2 + a_2 + a_1)^3 - (2b_1 + a_2 + a_1)^3\right]}{6*L*\pi^2*n^2} \end{aligned} \tag{3.89}$$

The real part value is the spring stiffness (k) of air, the imaginary part value is the damping (b) of air. The stiffness of air underneath tilting plate is the spring component of the reaction force divided by the tip displacement.

$$\begin{aligned} k_{spring} &= \tau(t)/H' \\ &= Re\left[\sum_{n=even} P_a \frac{-j\omega e^{j\omega t}}{j\omega + k^2{}_{mn}/a^2} \times \frac{\sqrt{2}\mathrm{a}^3\mathrm{b}}{L*\pi^2*n^2} + \sum_{n=odd} P_a \frac{-jwe^{jwt}}{jw + k^2{}_{mn}/a^2} \times \frac{\sqrt{2}\mathrm{a} \times \left[(2b_2 + a_2 + a_1)^3 - (2b_1 + a_2 + a_1)^3\right]}{6*L*\pi^2*n^2}\right] \end{aligned} \tag{3.90}$$

Similarly, the damping coefficient of air underneath tilting plate can be determined from the damping component of the reaction force divided by the tip velocity:

$$b_{damping} = \tau(t)/v$$

$$= Im[\sum_{n=even} P_a \frac{-je^{j\omega t}}{j\omega + k^2{}_{mn}/a^2} \times \frac{\sqrt{2}\mathrm{a}^3\mathrm{b}}{L*\pi^2*n^2} + \sum_{n=odd} P_a \frac{-je^{jwt}}{jw + k^2{}_{mn}/a^2} \times \frac{\sqrt{2}\mathrm{a} \times \left[(2b_2 + a_2 + a_1)^3 - (2b_1 + a_2 + a_1)^3\right]}{6*L*\pi^2*n^2}] \quad (3.91)$$

Compare the frequency responses of analytical and COMSOL

After building the analytical equation of all four elements, the analytical model of tilting plate with a hole in the center can be got. According to the restoring torque of the three elements showed above, the k_{air} and b_{air} are all corresponding to the maximum z displacement occurring at the tip of $(\frac{a}{2}, \frac{a}{2})$ and $(-\frac{a}{2}, -\frac{a}{2})$. So it is reasonable to get the $k_{total,air}$ and $b_{total,air}$ by add k_{air} and b_{air} of each elements together. As showing in Figure 3.19, the tilting plate has 8 elements which are combined by 2 of element 'A', 2 of element 'B', 2 of element 'C' and 2 of element 'D'. The total air stiffness and air damping can be expressed as:

$$k_{total,air} = 2k_a + 2k_b + 2k_c + 2k_d \quad (3.92)$$

$$b_{total,air} = 2b_a + 2b_b + 2b_c + 2b_d \quad (3.93)$$

As before, the mass moment of inertia (I) can be calculated by:

$$I = \frac{1}{12} m_{big} a^2 - \frac{1}{12} m_{small} s^2 \quad (3.94)$$

Where $m_{big}$is the mass of the original plate is, a is the length of the original plate. And m_{small} is the mass of the square hole plate, s is the length of the plate as a hole.

The same transfer function showed in regular tilting plate, the frequency response of the tilting plate with a hole can be got.

$$\frac{\theta(t)}{\tau(t)} = \sqrt{\frac{1}{\left((k_{flex} + k_{air,total}(\omega)) - I \times \omega(t)^2\right)^2 + \left(b_{air,total}(\omega) \times \omega(t)\right)^2}} \quad (3.95)$$

Then, the analytical frequency response of the tilting plate can be calculated with MATLAB by using the parameters shown in Table 3.4.

Table 3. 4: Parameter used in both analytical and simulated tilting plate models

Pa	101000 Pa
$\mu_{effective}$	1.862×10^{-5} Pa.s
L	200 µm
W	200 µm
t	3 µm
ρ	2330 kg/m^3
g_0	4 µm
k_{flex}	$6 \times 10^{-8} Nm/rads$
s (hole size)	50 µm × 50 µm

Simulated model in COMSOL MULTIPHYSICS

Sketch a tilting plate in COMSOL MULTIPHYSICS by using the parameters the same as in analytical model. As the plate was assembled by 8 elements, make sure add a wall between each element connecting edges, make sure the flow rate cross the edges equal to zero so that no air cross that edges, it satisfied the same boundary condition assumption as in the analytical model.

Figure 3.20 shows the air damping pressure distribution in COMSOL of 200 μm × 200 μm tilting plate with a 50 μm × 50 μm hole in the center. The highest air damping pressure occurs at the two adjacent edges closed element. This is reasonable because this element experiences the largest compression displacement and no air cross that edge.

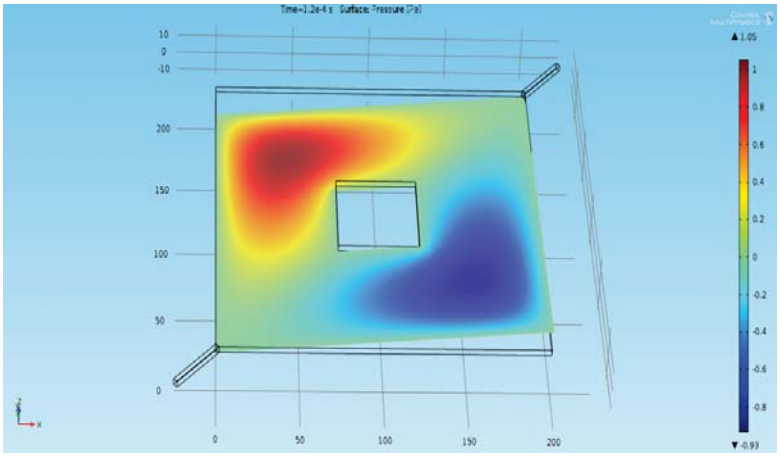

Figure 3.20: The air damping pressure distribution on surface

Figure 3.21 shows the frequency response by Frequency (rad/s) versus Magnitude Ratio. This tilting plate is a 200(um) × 200(um) square plate with a 50(um) × 50(um) hole in the center. The results indicate that the analytical model matches the simulation very well. Three more models are built in order to identify the analytical model.

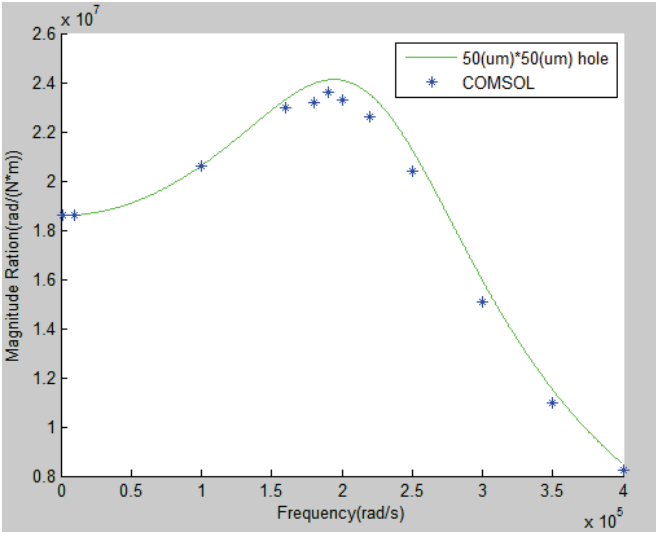

Figure 3.21: The frequency response of tilting plate about its diagonal with a hole

Figure 3.22 shows additional comparisons for different hole size tilting plates. The results indicate that the analytical model matches the simulation very well. This analytical model can be used to do design optimization.

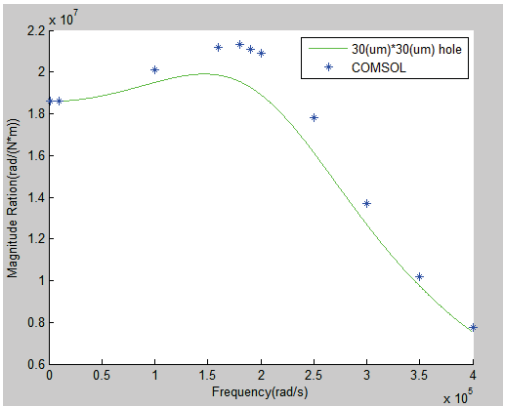

(a)

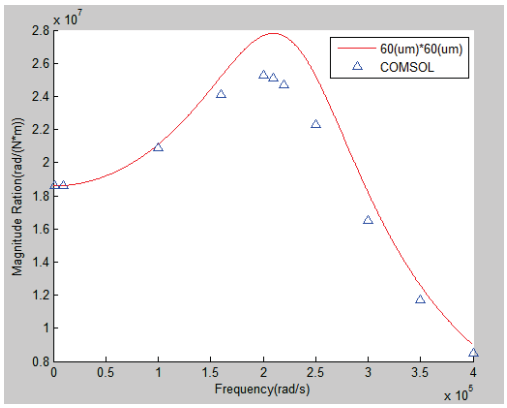

(b)

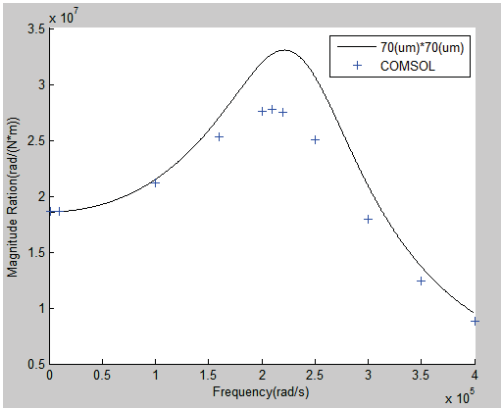

(c)

Figure 3.22: The 200(um) *200(um) tilting plate with different hole size in the center

3.3 Optimization of both tilting plates

The vapor sensor is covered by a chemical coating, which is used to absorb the particular chemical vapor molecules. The mass of the tilting plate will increase due to the absorbed chemical vapor. The goal is find the optimum hole size which has low air damping force and large chemical coating area for absorbing the chemical vapor. In order to simplify the calculation, Miller and Li [21] defined a new measure Q_S, which is just need two points of the root mean square deviation (RMSD) measurement. It is expressed as below:

$$Q_S = \sqrt{\frac{(M_{ab}^r - M_{no})^2 + (M_{no}^r - M_{ab})^2}{(M_{no})^2 + (M_{ab})^2}} \times 100\% \qquad (3.96)$$

Where M_{ab}^{r} and M_{no}^{r} are the magnitude ratio at the resonant frequencies of the absorbed mass system and without absorb system, respectively. Figure 3.23 shows the frequency responses for two different systems with and without absorb chemical vapor mass. And also shows the parameters in the previous equation.

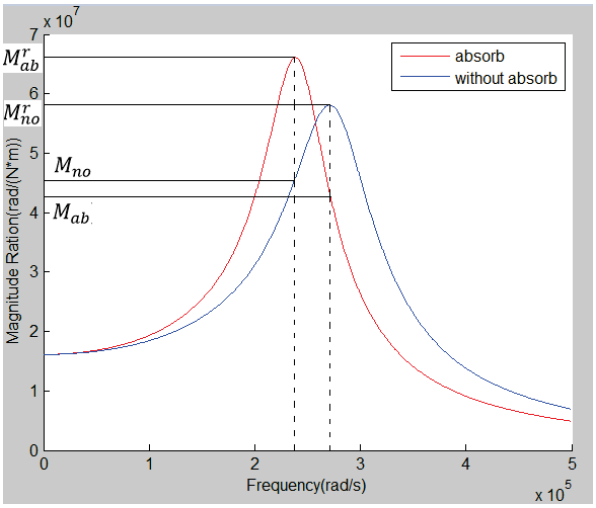

Figure 3.23: The parameter definitions of Q_S

The tilting plate is coated with a polymer chemical coating that will absorb the particular chemical vapor. For example, in [17], the plate is coated by PPEOsNa+ polymer to absorb nerve gas analog (DMMP). The DMMP will be absorbed approximately 5.6 *mg/m*^{2} by 100 *nm* thick polymer coating. Because the coating area corresponds to the tilting plate area, in this case, I assume that the absorbed chemical vapor adds 10% to the mass of the plate. This thesis is focus on how the hole size will influence the Qs of tilting plate. The table 3.5 below shows the parameters that used in the optimization design of both tilting plate.

Table 3. 5: Parameters used in both tilting plate models.

Pa	101000 Pa
$\mu_{effective}$	1.862× 10^{-5} Pa.s
L	200 µm
W	200 µm
t	3 µm
ρ	2330 kg/m^3
g_0	4 µm
k_{flex}	$6.2 \times 10^{-8} Nm/rads$
$b_{material}$	1×10^{-14} $Nms/rads$

In the transfer function equation for the tilting plate with a hole in the center, MR_{ab} and MR_{no} represents the magnitude ratio with 10% chemical vapor mass absorption and without chemical mass absorption, respectively.

$$MR_{ab} = \frac{\theta(t)}{\tau(t)} = \sqrt{\frac{1}{\left(\left(k_{flex} + k_{air,total}(\omega)\right) - I \times (1 + 10\%) \times w(t)^2\right)^2 + \left((b_{air,total}(\omega) + (b_{material}) \times w(t)\right)^2}}$$

$$MR_{no} = \frac{\theta(t)}{\tau(t)} = \sqrt{\frac{1}{\left(\left(k_{flex} + k_{air,total}(\omega)\right) - I \times w(t)^2\right)^2 + \left((b_{air,total}(\omega) + (b_{material}) \times w(t)\right)^2}}$$

Figure 3.24 shows how the Q_S change with different hole size of tilting plate about *y* axis. The highest Q_S is 73% with the hole size of 170 μm.

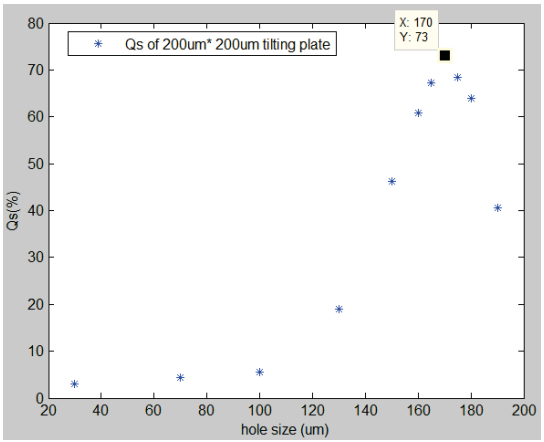

Figure 3.24: Sensor sensitivity Q_S with different hole size for tilting plate about y axis

Figure 3.25 shows how the Q_S change with different hole size of tilting plate about diagonal. The highest Q_S is 68.42% with the hole size of 170 μm.

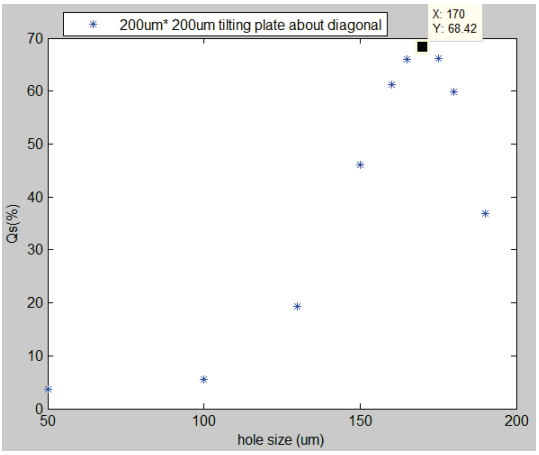

Figure 3.25: Sensor sensitivity Q_S with different hole size for tilting plate about diagonal

Compared the tilting plate about *y* axis, tilting plate about diagonal in terms of Q_S. In the same situation with the 10% mass is added to the entire surface of the model, tilting plate about y axis model gives the highest Q_S value which is 73%, tilting plate about diagonal gives Q_S value of 68%. The reason is that for the same size plate, tilting about diagonal has more damping force than tilting about *y* axis.

3.4 Optimization based on capacitance to voltage

The frequency response discussed above does not relate to the electronic actuation force and capacitance sensing area. The magnitude ratio is calculated by dividing a rotation angle by a torque, or $\frac{d\theta}{d\tau}$. For an electronic actuated with capacitance sensing resonant mass sensor, the input should be voltage, and the output should be capacitance. The magnitude ratio of interest is $\frac{dC}{dV}$. According to [17], this new magnitude ratio can be found from:

$$\frac{dC}{dV} = \frac{d\theta}{d\tau}\frac{dC}{d\theta}\frac{d\tau}{dV} \tag{3.97}$$

Figure 3.26 shows the tilting plate is oscillated with small rotation about an offset angle θ, which is caused by a DC offset voltage V_0. For the lowest energy consumption, the electrostatic voltage should be close to the free edge with the smallest gap. Therefore, the red area is used for capacitance, and the green area is used for actuating.

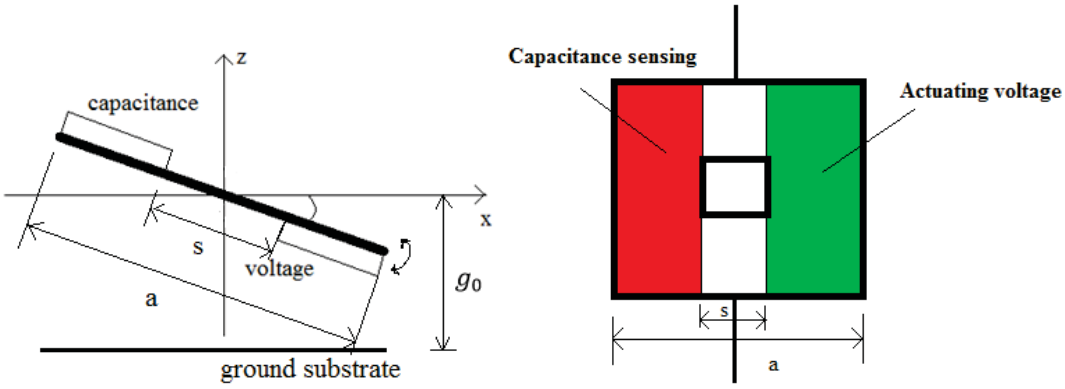

Figure 3.26: Sensing and actuating area in tilting plate with a hole in the center

The equation for capacitance is:

$$dC = \frac{\varepsilon dA_s}{g_0 + tan\theta \times x} \tag{3.98}$$

Where A_s is the capacitance area, ε is the permittivity of air, g_0 is the gap between actuator and substrate. Because θ is a small angle, so that $tan\theta = \theta$. $dA_s = W_a \times dx$. Where W_a is the width of the tilting plate.

$$dC = \frac{\varepsilon W dx}{g_0 + \theta x} \tag{3.99}$$

The domain of the capacitance area is $-\frac{a}{2} < x < -\frac{s}{2}$, The equation for the capacitance force is:

$$C = \int_{-\frac{a}{2}}^{-\frac{s}{2}} \frac{\varepsilon W_a}{g_0 + \theta x} dx$$

$$= \int_{-\frac{a}{2}}^{-\frac{s}{2}} \frac{\varepsilon W_a}{g_0 + \theta x} dx$$

$$= \frac{\varepsilon W_a}{\theta} \log(g_0 + \theta x)_{-\frac{a}{2}}^{-\frac{s}{2}} \tag{3.100}$$

$$C = \frac{\varepsilon W_a}{\theta} \left(\log(g_0 - \theta \frac{s}{2}) - \log(g_0 - \theta \frac{a}{2}) \right) \tag{3.101}$$

Where a is the length of tilting plate, and s is the length of the hole.

In order to obtain an expression for $\frac{dC}{d\theta}$, differentiating the *C* equation:

$$\frac{dC}{d\theta} = \frac{d\left(\frac{\varepsilon W_a}{\theta}\left(\log(g_0-\theta\frac{s}{2})-\log(g_0-\theta\frac{a}{2})\right)\right)}{d\theta}$$

$$= \varepsilon W_a\left(\frac{\frac{a\theta}{2g_0+a\theta}-\log\left(g_0+\theta\frac{a}{2}\right)-\frac{s\theta}{2g_0+s\theta}+\log\left(g_0+\theta\frac{s}{2}\right)}{\theta^2}\right) \quad (3.102)$$

The domain of the actuating area is $\frac{s}{2} < x < \frac{a}{2}$, the equation for the actuating area is showing blow.

$$dF = \frac{\varepsilon V^2 dA_a}{2(g_0-\theta x)^2} \quad (3.103)$$

Where A_a is the actuating area, ε is the permittivity of air, g_0 is the gap between actuator and substrate. And $dA_a = W \times dx$. Where W is the width of the tilting plate. Then converting the force to torque:

$$\tau_a = \int x dF = \int_{\frac{s}{2}}^{\frac{a}{2}} \frac{\varepsilon V^2 W_a x}{2(g_0-\theta x)^2}\, dx$$

$$= \frac{\varepsilon V^2 W_a}{2}\int_{\frac{s}{2}}^{\frac{a}{2}} \frac{x}{(g_0-\theta x)^2}\, dx$$

$$= \frac{\varepsilon V^2 W_a}{2\theta^2}\left(\frac{g_0}{g_0-\theta x} + \log(g_0-\theta x)\right)_{\frac{s}{2}}^{\frac{a}{2}} \quad (3.104)$$

$$\tau_a = \frac{\varepsilon V^2 W_a}{2\theta^2}\left(\frac{g_0}{g_0-\theta\frac{a}{2}} + \log\left(g_0-\theta\frac{a}{2}\right) - \frac{g_0}{g_0-\theta\frac{s}{2}} - \log\left(g_0-\theta\frac{s}{2}\right)\right) \quad (3.105)$$

Where a is the length of tilting plate, and *s* is the length of the hole. This equation indicates that the angle θ is dependent by the hole size s. The tilting plate with different size hole, it will have different offset angle.

In order to obtain an expression for $\frac{d\tau}{dV}$, substitute $\theta = \frac{\tau}{k}$ into the equation shows above.

$$\varepsilon V^2 W_a\left(\frac{g_0}{g_0-\theta\frac{a}{2}} + \log\left(g_0-\theta\frac{a}{2}\right) - \frac{g_0}{g_0-\theta\frac{s}{2}} - \log\left(g_0-\theta\frac{s}{2}\right)\right) = 2k\theta^3$$

$$\varepsilon V^2 W_a\left(\frac{g_0}{g_0-\frac{\tau a}{k2}} + \log\left(g_0-\frac{\tau}{k}\frac{a}{2}\right) - \frac{g_0}{g_0-\frac{\tau s}{k2}} - \log\left(g_0-\frac{\tau}{k}\frac{s}{2}\right)\right) = 2k\left(\frac{\tau}{k}\right)^3 \quad (3.106)$$

Differentiating this equation gives:

$$\frac{2\tau^2\left(\frac{2g_0k\tau(a-s)(-8g_0k\tau(a+s)+5as\tau^2+12{g_0}^2k^2)}{(a\tau-2g_0k)^2(s\tau-2g_0k)^2}+3\log\left(g_0-\frac{a\tau}{2k}\right)-3\log\left(g_0-\frac{s\tau}{2k}\right)\right)}{k^2\left(2g_0k\left(\frac{1}{a\tau-2g_0k}+\frac{1}{2g_0k-s\tau}\right)-\log\left(g_0-\frac{a\tau}{2k}\right)+\log\left(g_0-\frac{s\tau}{2k}\right)\right)^2}d\tau = 2V\varepsilon W_a dV$$

$$\frac{d\tau}{dV}=\frac{2V\varepsilon W_a k^2\left(2g_0k\left(\frac{1}{a\tau-2g_0k}+\frac{1}{2g_0k-s\tau}\right)-\log\left(g_0-\frac{a\tau}{2k}\right)+\log\left(g_0-\frac{s\tau}{2k}\right)\right)^2}{2\tau^2\left(\frac{2g_0k\tau(a-s)(-8g_0k\tau(a+s)+5as\tau^2+12{g_0}^2k^2)}{(a\tau-2g_0k)^2(s\tau-2g_0k)^2}+3\log\left(g_0-\frac{a\tau}{2k}\right)-3\log\left(g_0-\frac{s\tau}{2k}\right)\right)} \quad (3.107)$$

Substitute $\frac{\tau}{k}=\theta$ into the equation shows above. At the set point of $V_0\ and\ \tau_0$, the slope is:

$$\frac{d\tau}{dV}=\frac{2V\varepsilon W_a\left(2g_0\left(\frac{1}{a\theta-2g_0}+\frac{1}{2g_0-s\theta}\right)-\log\left(g_0-\frac{a}{2}\theta\right)+\log\left(g_0-\frac{s}{2}\theta\right)\right)^2}{2\theta^2\left(\frac{2g_0\theta(a-s)(-8g_0\theta(a+s)+5as\theta^2+12{g_0}^2)}{(a\theta-2g_0)^2(s\theta-2g_0)^2}+3\log\left(g_0-\frac{a}{2}\theta\right)-3\log\left(g_0-\frac{s}{2}\theta\right)\right)} \quad (3.108)$$

For the rotational angle to the torque, the transfer function is:

$$\frac{d\theta}{d\tau}=\frac{1}{ms_t^2+bs_t+k} \quad (3.109)$$

Combining these three equations,

$$\frac{dC}{dV}=\frac{d\theta}{d\tau}\frac{dC}{d\theta}\frac{d\tau}{dV}=\frac{1}{ms_t^2+bs_t+k}\times\varepsilon W_a\left(\frac{\frac{a\theta_0}{2g_0+a\theta_0}-\log\left(g_0+\theta_0\frac{a}{2}\right)-\frac{s\theta_0}{2g_0+s\theta_0}+\log\left(g_0+\theta_0\frac{s}{2}\right)}{{\theta_0}^2}\right)$$

$$\times\frac{2V\varepsilon W_a\left(2g_0\left(\frac{1}{a\theta_0-2g_0}+\frac{1}{2g_0-s\theta_0}\right)-\log\left(g_0-\frac{a}{2}\theta_0\right)+\log\left(g_0-\frac{s}{2}\theta_0\right)\right)^2}{2{\theta_0}^2\left(\frac{2g_0\theta_0(a-s)\left(-8g_0\theta_0(a+s)+5as{\theta_0}^2+12{g_0}^2\right)}{(a\theta_0-2g_0)^2(s\theta_0-2g_0)^2}+3\log\left(g_0-\frac{a}{2}\theta_0\right)-3\log\left(g_0-\frac{s}{2}\theta_0\right)\right)} \quad (3.110)$$

According to this equation, $\frac{dC}{d\theta}\frac{d\tau}{dV}$ depends on the hole size s. As mentioned before, it's more efficient if the actuating area is close to the free edge near the substrate (assuming an offset voltage is applied). Therefore, assuming that the actuation area and sensing area are constant and not dependent on hole size, then the variable $'s'$ in previous equation is a constant. Then $\frac{dC}{d\theta}\frac{d\tau}{dV}$ is a constant. It indicates that the frequency response for $\frac{d\theta}{d\tau}$ differs from $\frac{dC}{dV}$ only by a constant multiple. Therefore, it will not influence the Qs shape in previous section.

CHAPTER IV: Resonant Mass Sensor Design Based on Fixed-Free Cantilever

4.1 Fixed-Free micro-cantilever without hole

The fixed-free micro-cantilever structure is a common resonator design, and it is strongly impacted by squeeze film compressive damping. This section derives an analytical squeeze film damping model of a micro-cantilever according to the Green's function approach [22]. The fixed-free cantilever with no hole can be represented with the model shown in Figure 4.1. The electrostatic actuating force is assumed to be a concentrated force at the tip.

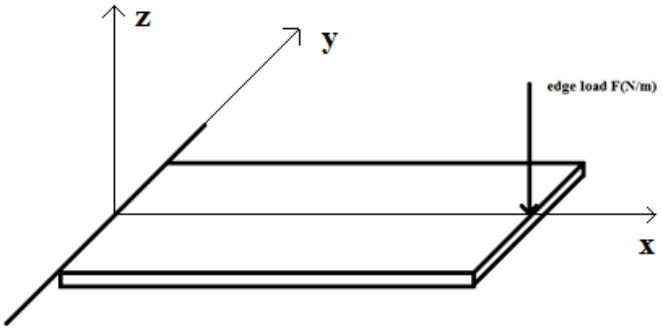

Figure 4.1: The fixed-free micro-cantilever without hole

According to the Green's function, the net reaction force is calculated as

$$F(t) = abP_a \sum_{\substack{m=odd \\ n=odd}} \frac{64}{\pi^4 m^2 n^2} \left(1 - \frac{8}{\pi^2 m^2}\right)^2 \frac{-j\omega\eta H' e^{j\omega t}}{j\omega + {k_{mn}}^2/\alpha^2} \tag{4.1}$$

For *m*, *n= {1, 3, 5……}*, and the corresponding eigenvalues are

$$k_{mn} = \frac{m^2\pi^2}{4a^2} + \frac{n^2\pi^2}{b^2} \tag{4.2}$$

Where ω is the vibration frequency, Pa is the ambient pressure, a and b are the length and width of the cantilever, respectively. The length of a is the plate dimension in the direction of bending. The "H'" is the normalized maximum deflection of the cantilever at the free-end. Based on the isothermal condition, the $\eta = 1$. According to the squeeze number function, $\alpha^2 = \frac{12\mu}{\eta {h_0}^2 P_a}$ where μ is the viscosity of air.

The real part value is the spring stiffness (k) of air and the imaginary part value is the damping (b) of air. The stiffness of air is the spring component of the reaction force divided by the tip displacement.

$$k_{spring} = F(t)/H'$$

$$= abP_a \times \mathrm{Re}\left[\sum_{\substack{m=odd \\ n=odd}} \frac{64}{\pi^4 m^2 n^2} \left(1 - \frac{8}{\pi^2 m^2}\right)^2 \frac{-j\omega\eta e^{j\omega t}}{j\omega + {k_{mn}}^2/\alpha^2}\right] \tag{4.3}$$

The damping coefficient of air underneath a cantilever can be determined by the damping component of the reaction force divided by the tip velocity:

$$b_{damping} = F(t)/v$$
$$= abP_a \times \text{Imag}[\sum_{\substack{m=odd \\ n=odd}} \frac{64}{\pi^4 m^2 n^2}(1 - \frac{8}{\pi^2 m^2})^2 \frac{-j\omega\eta e^{j\omega t}}{j\omega + {k_{mn}}^2/\alpha^2}] \quad (4.4)$$

After obtaining the stiffness and damping coefficient of air, the analytical model can be built. As mentioned before, the electrostatic force is assumed as a concentrated load at the free end of the cantilever as shown in Figure 4.2.

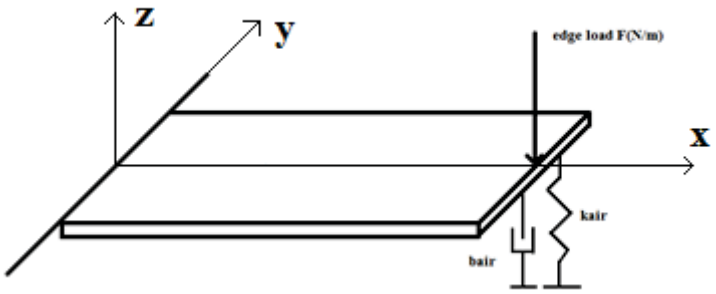

Figure 4.2: The free body diagram of cantilever

According to Newton's Second Law and the free body diagram, the equation of motion is:

$$F(t) = m\ddot{v} + b\dot{v} + kv \quad (4.5)$$

The transfer function can be expressed as:

$$\frac{V(s)}{F(x)} = \frac{1}{ms^2 + bs + k} \quad (4.6)$$

Where *m* is the effective mass of the cantilever, *b* is the damping coefficient of air, and *k* is the sum of stiffness of material and air. $k = k_{flex} + k_{air}$. *V(s)* is the maximum displacement at the free end of the cantilever and *F(s)* is the maximum sinusoid force, where $\frac{V(s)}{F(s)}$ is the magnitude ratio.

Substitute *s=jw* into the transfer function, the magnitude ratio was calculated by:

$$\left|\frac{V(j\omega)}{F(j\omega)}\right| = \frac{1}{|(k - m\omega^2) + (b\omega)j|} = \frac{1}{\sqrt{(k(\omega) - m\omega^2)^2 + (b(\omega)\omega)^2}} \quad (4.7)$$

Because the sinusoid force was applied at the free end of cantilever, the stiffness of material should be calculated by the equation:

$$k = \frac{3EI}{L^3} \quad (4.8)$$

Where L is the length of the cantilever, E is the young's modulus which is equal to 170×10^9 P_a due to the property of silicon. I is the moment of inertia of the cantilever, which equals to $\frac{b*h^3}{12}$, where b is the width and h is the height of the cantilever. The effective mass can be calculated by the equation shown below:

$$\omega = \left(\frac{1.875}{L}\right)^2 \sqrt{\frac{EI}{\rho A}} \tag{4.9}$$

$$\omega = \sqrt{\frac{k}{m_{eq}}} \tag{4.10}$$

Where ω is the resonant frequency of the cantilever, A is the cross-section area and k is the stiffness of the cantilever. We can then get the effective mass.

The analytical frequency response of the cantilever was calculated with MATLAB using the parameters shown in Table 4.1.

Table 4. 1: Parameter used in cantilever without hole

Pa	101000 Pa
$\mu_{effective}$	1.862× 10^{-5} Pa.s
L	300 µm
W	50 µm
t	3 µm
ρ	2330 kg/m^3
g_0	4 µm

Simulated model in COMSOL MULTIPHYSICS

The procedure for creating a simulation model in COMSOL was the following:

1. Choose the solid mechanics physics and time dependent model to sketch a 300 um × 50 um × 3 um cantilever.
2. Set the thin-film damping on the bottom surface of the cantilever with a gap of 4 um, the ambient pressure is 1 atmospheric pressure and the viscosity of air is 22.6×10^{-6} $Pa.s$ in a room temperature of 293.15 K.
3. The material of the cantilever is silicon.
4. Apply the sinusoidal load $1 \times 10^{-2} \times \sin(\omega \times t)$ N/m at the free edge of the cantilever. Make sure the deflection will be in the elastic region, and make sure the tip deflection is smaller than the gap.
5. Collect each tip displacement value at the free edge in different frequencies. From that, the magnitude ratio is equal to the tip displacement divided by the total edge load.

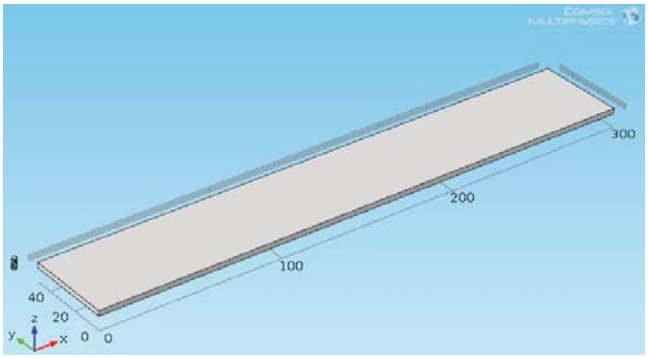

Figure 4.3: Micro-cantilever model was built in COMSOL

Figure 4.4 shows the mesh for the COMSOL model. Again, the 'Free Tetrahedral' element can be used. According to the test, mesh dimension of 'Coarse' is sufficient for the mesh optimization. This model has more than 5000 elements; it takes 10-15 minutes to get one frequency response point.

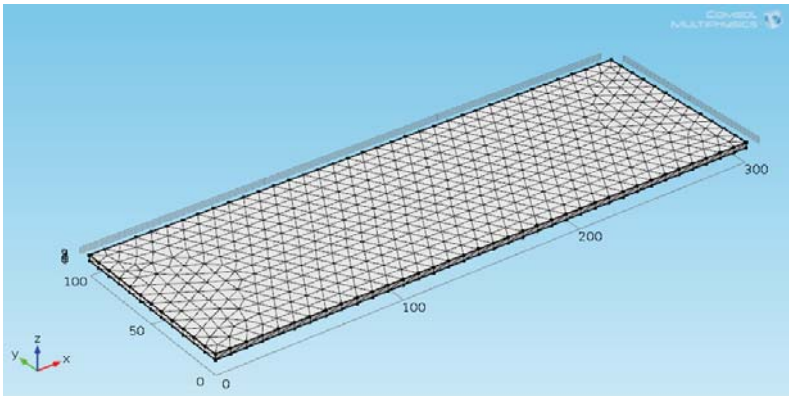

Figure 4.4: Mesh of cantilever is COMSOL

Figure 4.5 compares the frequency responses between the analytical and COMSOL models. The analytical result is close to the simulation results. Like before, the analytical model outputs a result in just 1 minute, and each point of the simulation result requires at least 10 minutes running time.

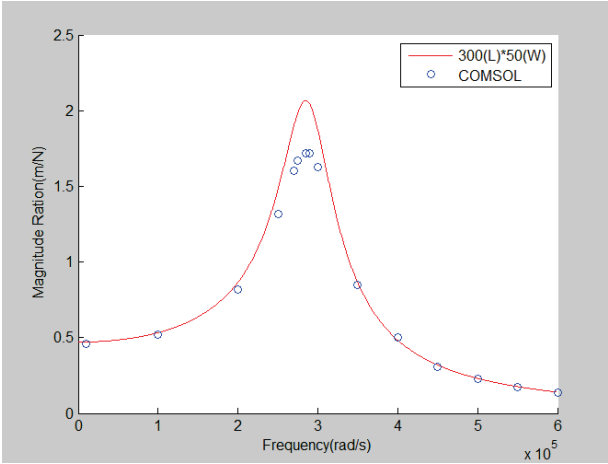

Figure 4.5: The frequency response of cantilever without hole

Figure 4.6 shows additional comparisons for different sized cantilever. The results indicate that the analytical model matches the simulation very well. As mentioned before, the air damping will influence the magnitude ratio; the magnitude ratio at the resonant frequency increases when the air damping decreases. Figure 4.6 shows that with the same length of $300\mu m$, narrowing the cantilever reduces the air damping. But more areas are needed for actuation, sensing and also absorb the chemical materials. Therefore, add a hole in tilting plate is a more efficient way to reduce air damping.

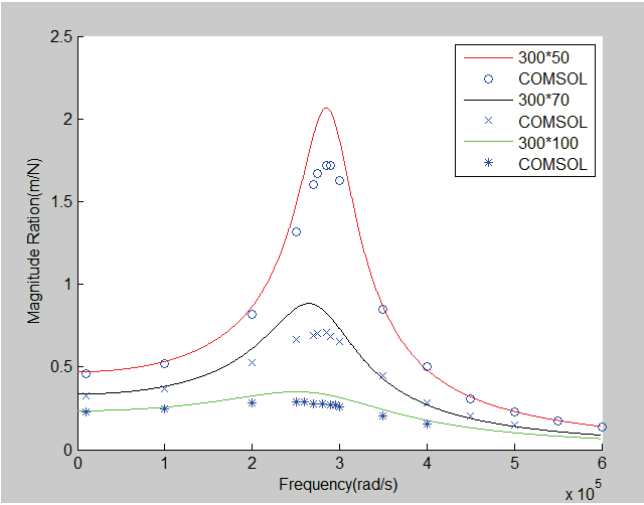

Figure 4.6: The frequency responses of different sized cantilevers

4.2 Fixed- Free micro-cantilever with a hole in the center

In order to reduce the air damping, a square hole was added in the center of the cantilever. As shown in Figure 4.7, the cantilever was divided into 8 small plates with five kinds of elements in total. Element 'A' has two adjacent edges closed, Element 'B1' has two opposite edges closed along the y axis and element 'B2' has two opposite edges closed along the x axis. Element 'C1' has three edges closed but venting along the y axis, element 'C2' has three edges closed but venting along the x axis. According to the element equations with different boundary conditions [22], the analytical equation of each element shown in Figure 4.7 can be obtained.

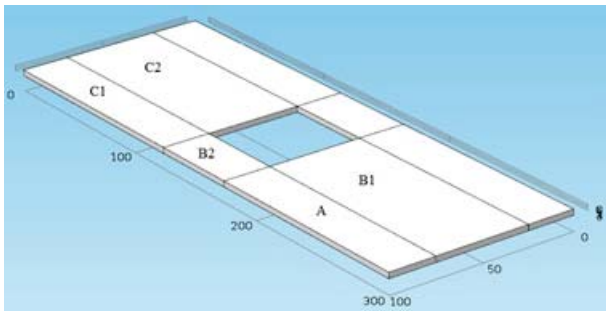

Figure 4.7: The cantilever with a hole in the center model in COMSOL

The cantilever is fixed at the left side with the maximum displacement in *z* direction occurring at the right edges. The normalized displacement of the plate can be described as

$$H(x,y,t) = H'(\frac{x}{L})^2 e^{j\omega t} \tag{4.11}$$

Where L is the length of the cantilever and H' is the maximum displacement at the free end.

4.2.1 Element 'A' with two adjacent edges closed

The domain of the compressed area of element 'A' in Figure 4.7 has two adjacent edges closed. To derive the analytical equation of element 'A', begin with the equation for the regular cantilever with two adjacent edges closed as shown in Figure 4.8. The integral procedure is the same as the cantilever shown above. The only things changed are the eigenfunctions and corresponding eigenvalues corresponding to different boundary conditions. The domains of element 'A' are taken to be $0 < x < a$, $-\frac{b}{2} < y < \frac{b}{2}$, corresponding to a rectangular cantilever of dimensions $a \times b$. The two adjacent edges

closed are expressed as $\frac{\partial P}{\partial y} = 0$ at $y = \frac{b}{2}$, and $\frac{\partial P}{\partial x} = 0$ at $x = 0$, with ideal venting $P=0$ along the remaining two edges of $x = a$ and $y = -\frac{b}{2}$.

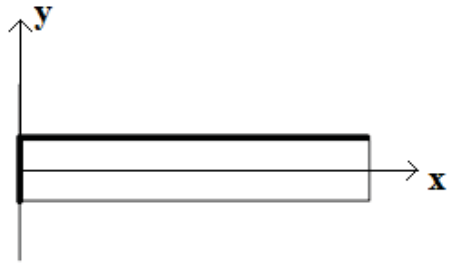

Figure 4.8: The micro-cantilever with two adjacent edges closed

The eigenfunctions are:

$$u_{mn}(x,y) = \sqrt{\frac{4}{ab}}\cos\frac{m\pi}{2a}(x) * \cos\frac{n\pi}{2b}\left(y + \frac{b}{2}\right) \tag{4.12}$$

Where *m, n = {1,3,5…..}*. The associated eigenvalues are

$$k_{mn} = \frac{m^2\pi^2}{4a^2} + \frac{n^2\pi^2}{4b^2} \tag{4.13}$$

The concentrated force at the tip of the plate can be expressed as:

$$F(t) = \sum_{\substack{m=odd \\ n=odd}} Pa \frac{-j\omega H' e^{j\omega t}}{j\omega + k^2{}_{mn}/a^2} * \frac{64\text{ab}}{\pi^8 m^6 n^2} * (\pi^2 m^2 - 8)^2 \tag{4.14}$$

The real part is the spring stiffness (*k*) of air, and the imaginary part value is the damping (*b*) of air. The stiffness of air underneath cantilever is the spring component of the reaction force divided by the tip displacement.

$$k_{spring} = F(t)/H'$$

$$= \text{Re}\left[\sum_{\substack{m=odd \\ n=odd}} Pa \frac{-j\omega e^{j\omega t}}{j\omega + \frac{k^2_{mn}}{a^2}} * \frac{64\text{ab}}{\pi^8 m^6 n^2} * (\pi^2 m^2 - 8)^2\right] \tag{4.15}$$

Similarly, the damping coefficient of air underneath cantilever can be determined from the damping component of the reaction force divided by the tip velocity:

$$b_{damping} = F(t)/v$$

$$= \text{Im}\left[\sum_{\substack{m=odd \\ n=odd}} Pa \frac{-j\omega e^{j\omega t}}{j\omega + \frac{k^2_{mn}}{a^2}} * \frac{64\text{ab}}{\pi^8 m^6 n^2} * (\pi^2 m^2 - 8)^2\right] \tag{4.16}$$

The magnitude ratio function shown below,

$$\left|\frac{V(j\omega)}{F(j\omega)}\right| = \frac{1}{|(k(\omega) - m\omega^2) + (b(\omega)\omega)j|} = \frac{1}{\sqrt{(k(\omega) - m\omega^2)^2 + (b(\omega)\omega)^2}} \tag{4.17}$$

Where *m* is the effective mass of the cantilever, b is the damping coefficient of air, and k is the sum of stiffness of material and air. *V(jω)* is the maximum displacement at the free

end of the cantilever and $F(j\omega)$ is the maximum sinusoid force, where $\frac{V(j\omega)}{F(j\omega)}$ is the magnitude ratio.

Simulated model in COMSOL

Build a 300 *um* × 50 *um* × 3 *um* cantilever in COMSOL as it is shown in the regular cantilever part. Create the boundary conditions "wall" at the two adjacent edges that can make sure no air cross those edges. It will satisfy the same boundary condition as two adjacent edges closed in the analytical model. Collect each maximum displacement value of the free edge in different frequencies. The simulated magnitude ratio is equal to the free end displacement X divided by the applied sinusoid force F.

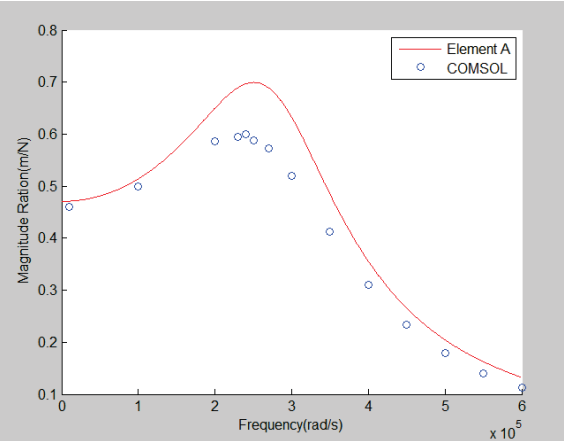

Figure 4.9: Regular cantilever 'A' with two adjacent edges closed

The simulate result and analytical result are fit good in Figure 4.9, that demonstrated that the analytical model of regular cantilever 'A' is worked. Then we can start to integral the analytical model of element 'A' showed in Figure 4.7.

The domain of the volume is taken to be $a_1 \leq x \leq a_2$ and $b_1 \leq y \leq b_2$, corresponding to a rectangular plate of dimensions $a \times b$, where $a = a_2 - a_1$ and $b = b_2 - b_1$. Plate 'A' has two adjacent edges closed, the boundary conditions can be expressed as $\frac{\partial P}{\partial x} = 0$ at $x = a_1$, and $\frac{\partial P}{\partial y} = 0$ at $y = b_1$. With venting $P=0$ along the other two edges of $x= a_2$ and $y= b_2$. According to these boundary conditions, the eigenfunctions become

$$u_{mn}(x,y) = \sqrt{\frac{4}{ab}} \cos\frac{m\pi}{2a}(x - a_1) * \cos\frac{n\pi}{2b}(y - b_1) \tag{4.18}$$

Where *m, n= {1,3,5…..}*. The associated eigenvalues are

$$k_{mn} = \frac{m^2\pi^2}{4a^2} + \frac{n^2\pi^2}{4b^2} \tag{4.19}$$

Following the approach described in Darling's paper, the normalized pressure distribution for this kind of plate can be derived as

$$P(x,y,t) = \sum_{\substack{m=odd \\ n=odd}} \frac{16(-1)^{\frac{n-1}{2}}}{\pi^4 m^3 n L^2} \frac{-j\omega H' e^{j\omega t}}{j\omega + k^2{}_{mn}/a^2} \left((\pi^2 m^2 a_2{}^2 - 8a^2)(-1)^{\frac{m-1}{2}} - 4\pi \mathrm{ama}_1 \right) * \cos\frac{m\pi}{2a}(x - a_1) * \cos\frac{n\pi}{2b}(y - b_1) \quad (4.20)$$

As the same integral way showed in Darling's paper, the concentrated force at the tip of the plate can be computed as:

$$F(t) = P_a \int_{a_1}^{a_2} \int_{b_1}^{b_2} (\frac{x}{L})^2 P(x,y,t) dxdy$$

$$= \sum_{\substack{m=odd \\ n=odd}} Pa \frac{-j\omega H' e^{j\omega t}}{j\omega + k^2{}_{mn}/a^2} * \frac{64\mathrm{ab}}{L^4 \pi^8 m^6 n^2} * \left((\pi^2 m^2 a_2{}^2 - 8a^2)(-1)^{\frac{m-1}{2}} - 4\pi \mathrm{ama}_1 \right)^2 \quad (4.21)$$

The stiffness of air underneath tilting plate is the real component of the reaction force divided by the tip displacement.

$$k_{spring} = F(t)/H'$$

$$= Re[\sum_{\substack{m=odd \\ n=odd}} Pa \frac{-j\omega e^{j\omega t}}{j\omega + k^2{}_{mn}/a^2} * \frac{64\mathrm{ab}}{L^4 \pi^8 m^6 n^2} * \left((\pi^2 m^2 a_2{}^2 - 8a^2)(-1)^{\frac{m-1}{2}} - 4\pi \mathrm{ama}_1 \right)^2] \quad (4.22)$$

Similarly, the damping coefficient of air underneath tilting plate can be determined from the imaging component of the reaction force divided by the tip velocity:

$$b_{damping} = F(t)/v$$

$$= Im[\sum_{\substack{m=odd \\ n=odd}} Pa \frac{-je^{j\omega t}}{j\omega + k^2{}_{mn}/a^2} * \frac{64\mathrm{ab}}{L^4 \pi^8 m^6 n^2} * \left((\pi^2 m^2 a_2{}^2 - 8a^2)(-1)^{\frac{m-1}{2}} - 4\pi \mathrm{ama}_1 \right)^2] \quad (4.23)$$

4.2.2 Plate ‘B1’ with two opposite edges closed along the y axis

The domain of the compressed area of element ‘B1’ in Figure 4.7 has two opposite edges closed along the y axis. Derive the analytical equation of element ‘B1’. Begin with the equation for the regular cantilever with two opposite edges closed as shown in Figure 4.10. The same integral procedure as shown in element ‘A’. The two adjacent edges closed are expressed as $\frac{\partial P}{\partial y} = 0$ at $y = \frac{b}{2}$, $y = -\frac{b}{2}$, with ideal venting P=0 along the remaining two edges of $x = 0$, $x = a$,

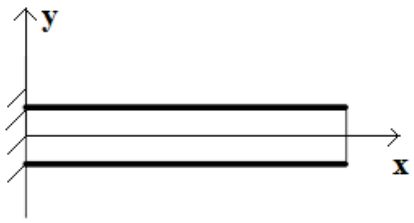

Figure 4.10: The micro-cantilever with two opposite edges closed along the *y* axis

The eigenfunction is:

$$u_{mn}(x,y) = \sqrt{\frac{2}{ab}} \cos sin \frac{n\pi}{a}(x - \frac{a}{2}) \tag{4.24}$$

Where *cos* is used for *n*= odd; *sin* is used for *n*= even. The corresponding eigenvalues are

$$k_{mn} = \frac{n^2\pi^2}{a^2} \tag{4.25}$$

Following the approach described in Darling’s paper, the normalized pressure distribution for this kind of plate can be derived as

$$P(x,y,t) = \sum_{n=odd} \frac{2}{\pi^3 n^3} \frac{-j\omega H' e^{j\omega t}}{j\omega + {k^2}_n/a^2} \left((\pi^2 n^2 - 4)(-1)^{\frac{n-1}{2}}\right) \times \cos\frac{n\pi}{a}\left(x - \frac{a}{2}\right) + \sum_{n=even} \frac{2}{\pi n} \frac{-j\omega H' e^{j\omega t}}{j\omega + {k^2}_n/a^2} (-1)^{\frac{n}{2}} \times \sin\frac{n\pi}{a}\left(x - \frac{a}{2}\right) \tag{4.26}$$

The concentrated force at the tip of the plate can be expressed as:

$$F(t) = \sum_{n=odd} Pa \frac{-j\omega H' e^{j\omega t}}{j\omega + \frac{k^2 n}{a^2}} * \frac{2ab}{\pi^6 n^6} * (\pi^2 n^2 - 4)^2 + \sum_{n=even} Pa \frac{-j\omega H' e^{j\omega t}}{j\omega + {k^2}_n/a^2} * \frac{2ab}{\pi^2 n^2} \tag{4.27}$$

The air stiffness and air damping can be known using force function. Then compared the simulate result with analytical result using magnitude ratio.

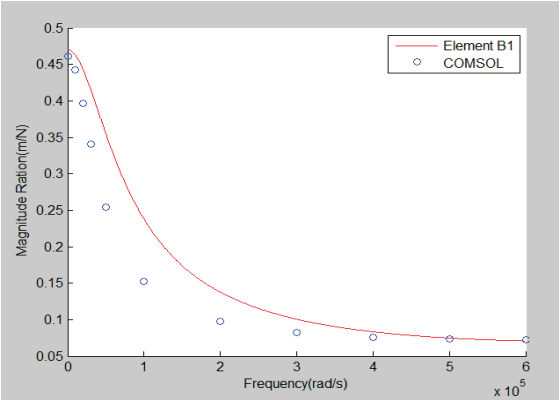

Figure 4.11: Regular cantilever 'B1' with two opposite edges closed along the y axis

The simulate result and analytical result are fit pretty good shown in Figure 4.11, that demonstrated that the analytical model of regular cantilever 'B1' is worked. Then we can start to integral the analytical model of element 'B1' showed in Figure 4.7.

The domain of the volume is taken to be $a_1 \leq x \leq a_2$ and $b_1 \leq y \leq b_2$, corresponding to a rectangular plate of dimensions $a \times b$, where $a = a_2\text{-}a_1$ and $b = b_2\text{-}b_1$. Element 'B1' has two opposite edges closed along the y axis, the boundary conditions can be expressed as $\frac{\partial P}{\partial y} = 0$ at $y= b_1$ and $y=b_2$. With venting $P=0$ along the other two edges of $x = a_1$ and $x = a_2$. According to these boundary conditions, the eigenfunctions become:

$$u_{mn}(x,y) = \sqrt{\frac{2}{ab}} \begin{matrix} cos \\ sin \end{matrix} \frac{n\pi}{a}(x - a') \tag{4.28}$$

Where *cos* is used for *n*= odd; *sin* is used for *n*= even. Here, $a' = \frac{(a_2+a_1)}{2}$. The associated eigenvalues are

$$k_n = \frac{n^2\pi^2}{a^2} \tag{4.29}$$

Following the approach described in Darling's paper, the normalized pressure distribution for this kind of plate can be derived as

$$P(x,y,t) = \sum_{m=odd} \frac{2}{\pi^3 m^3 L^2} \frac{-j\omega H' e^{j\omega t}}{j\omega + k^2_{mn}/a^2} \left(\pi^2 m^2 ({a_2}^2 + {a_1}^2) - 4a^2\right)(-1)^{\frac{n-1}{2}} * \cos\frac{n\pi}{a}(x - a') + \sum_{m=even} \frac{2}{\pi m L^2} \frac{-j\omega H' e^{j\omega t}}{j\omega + k^2_{mn}/a^2} ({a_1}^2 - {a_2}^2)(-1)^{\frac{n}{2}} * \sin\frac{n\pi}{a}(x - a') \tag{4.30}$$

As the same integral way showed in Darling's paper, the concentrated force at the tip of the plate can be computed as:

$$F(t) = P_a \int_{a_1}^{a_2} \int_{b_1}^{b_2} (\frac{x}{L})^2 P(x,y,t) dxdy$$

$$= \sum_{m=odd} Pa \frac{-j\omega H' e^{j\omega t}}{j\omega + k^2{}_{mn}/a^2} * \frac{2ab}{\pi^6 m^6 L^4} * \left(\pi^2 m^2 (a_2{}^2 + a_1{}^2) - 4a^2\right)^2 +$$

$$\sum_{m=even} Pa \frac{-j\omega H' e^{j\omega t}}{j\omega + k^2{}_{mn}/a^2} * \frac{2ab}{\pi^2 m^2 L^4} * (a_1{}^2 - a_2{}^2)^2 \quad (4.31)$$

The real part value is the spring stiffness (k) of air, the imaginary part value is the damping (b) of air. The stiffness of air underneath cantilever is the spring component of the reaction force divided by the tip displacement.

$$k_{spring} = F(t)/H'$$

$$= Re[\sum_{m=odd} Pa \frac{-j\omega e^{j\omega t}}{j\omega + \frac{k^2 mn}{a^2}} * \frac{2ab}{\pi^6 m^6 L^2} * \left(\pi^2 m^2 (a_2{}^2 + a_1{}^2) - 4a^2\right)^2 +$$

$$\sum_{m=even} Pa \frac{-j\omega e^{jwt}}{j\omega + \frac{k^2 mn}{a^2}} * \frac{2ab}{\pi^2 m^2 L^4} * (a_1{}^2 - a_2{}^2)^2] \quad (4.32)$$

Similarly, the damping coefficient of air underneath cantilever can be determined from the damping component of the reaction force divided by the tip velocity:

$$b_{damping} = F(t)/v$$

$$= Re[\sum_{m=odd} Pa \frac{-je^{j\omega t}}{j\omega + \frac{k^2 mn}{a^2}} * \frac{2ab}{\pi^6 m^6 L^2} * \left(\pi^2 m^2 (a_2{}^2 + a_1{}^2) - 4a^2\right)^2 +$$

$$\sum_{m=even} Pa \frac{-je^{j\omega t}}{j\omega + \frac{k^2 mn}{a^2}} * \frac{2ab}{\pi^2 m^2 L^4} * (a_1{}^2 - a_2{}^2)^2] \quad (4.33)$$

4.2.3 Plate ‘B2’ with two opposite edges closed along the *x* axis

Begin with the equation for the regular cantilever with two opposite edges closed along the x axis as shown in Figure 4.12. The same procedure shows above. The two adjacent edges closed are expressed as $\frac{\partial P}{\partial x} = 0$ at $x= 0$, $x = a$, with ideal venting $P=0$ along the remaining two edges of $y = \frac{b}{2}$, $y = -\frac{b}{2}$,

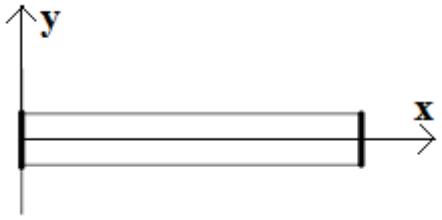

Figure 4.12: The micro-cantilever with two opposite edges closed along the *x* axis

The eigenfunction is:

$$u_{mn}(x,y) = \sqrt{\frac{2}{ab}} \begin{matrix}\cos \\ sin\end{matrix} \frac{n\pi}{b}(y) \tag{4.34}$$

Where *cos* is used for *n*= odd; *sin* is used for *n*= even. The associated eigenvalues are

$$k_{mn} = \frac{n^2\pi^2}{b^2} \tag{4.35}$$

Following the approach described in Darling’s paper, the normalized pressure distribution for this kind of plate can be derived as

$$P(x,y,t) = \sum_{n=odd} \frac{4x^2}{\pi n L^2} \frac{-j\omega H' e^{j\omega t}}{j\omega + k^2{}_{mn}/a^2} (-1)^{\frac{n-1}{2}} \cos\frac{n\pi}{b}(y) \tag{4.36}$$

The concentrated force at the tip of the plate can be computed as:

$$F(t) = P_a \int_{a_1}^{a_2} \int_{b_1}^{b_2} (\frac{x}{L})^2 P(x,y,t) dxdy$$

$$= \sum_{n=odd} \frac{8ab}{5\pi^2 n^2} \frac{-j\omega H' e^{j\omega t}}{j\omega + k^2{}_{mn}/a^2} \tag{4.37}$$

The air stiffness and air damping can be known using force function. Then compared the simulate result with analytical result using magnitude ratio.

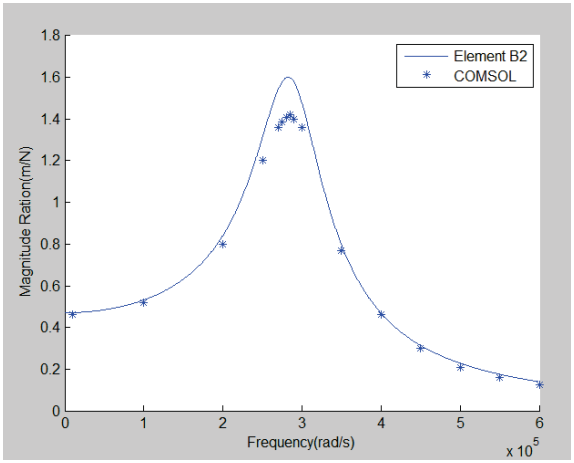

Figure 4.13: Regular cantilever 'B1' with two opposite edges closed along the x axis

The simulated result and analytical result match well as shown in Figure 4.13; that demonstrated that the analytical model of regular cantilever 'B2' works.

Then we can start to derive the analytical model of element 'B2' shown in Figure 4.7. The domain of the volume is taken to be $a_1 \leq x \leq a_2$ and $b_1 \leq y \leq b_2$, corresponding to a rectangular plate of dimensions a × b, where a = a_2-a_1 and b = b_2-b_1. The boundary conditions of element B2 can be expressed as $\frac{\partial P}{\partial x} = 0$ at $x = a_1$, and $x = a_2$. With venting P=0 along the other two edges of $y = b_1$ and $y = b_2$. The eigenfunctions becomes:

$$u_{mn}(x,y) = \sqrt{\frac{2}{ab}} \cos\frac{n\pi}{b}(y - b') \tag{4.38}$$

Where $n = \{1,3,5\ldots..\}$. Here, $b' = \frac{(b_2+b_1)}{2}$. The associated eigenvalues are

$$k_{mn} = \frac{n^2\pi^2}{b^2} \tag{4.39}$$

The normalized pressure distribution for this kind of plate can be derived as

$$P(x,y,t) = \sum_{\substack{m=even \\ n=odd}} \frac{4x^2}{\pi n L^2} \frac{-j\omega H' e^{j\omega t}}{j\omega + k^2{}_{mn}/a^2} (-1)^{\frac{n-1}{2}} \cos\frac{n\pi}{b}(y) \tag{4.40}$$

The concentrated force at the tip of the plate can be computed as:

$$F(t) = P_a \int_{a_1}^{a_2} \int_{b_1}^{b_2} (\frac{x}{L})^2 P(x,y,t)\,dx\,dy$$

$$= \sum_{\substack{m=even \\ n=odd}} \frac{8a^5 * b}{5\pi^2 n^2 L^4} \frac{-j\omega H' e^{jwt}}{j\omega + k^2{}_{mn}/a^2} \tag{4.41}$$

The stiffness of air underneath cantilever is the spring component of the reaction force divided by the tip displacement.

$$k_{spring} = F(t)/H'$$

$$= Re[\sum_{\substack{m=even \\ n=odd}} \frac{8a^5 * b}{5\pi^2 n^2 L^4} \frac{-j\omega H' e^{j\omega t}}{j\omega + k^2{}_{mn}/a^2}] \quad (4.42)$$

Similarly, the damping coefficient of air underneath cantilever can be determined from the damping component of the reaction force divided by the tip velocity:

$$b_{damping} = F(t)/v$$

$$= Im[\sum_{\substack{m=even \\ n=odd}} \frac{8a^5 * b}{5\pi^2 n^2 L^4} \frac{-j\omega e^{j\omega t}}{j\omega + k^2{}_{mn}/a^2}] \quad (4.43)$$

4.2.4 Plate 'C1' with three edges closed but venting along the y axis

As shown in Figure 4.14, the derivation begins with the equation for the regular cantilever with three edges closed but venting along the *y* axis. The boundary condition can be expressed as $\frac{\partial P}{\partial x} = 0$ at $x = 0$, $x = a$, and $\frac{\partial P}{\partial y} = 0$ at $y = \frac{b}{2}$, with ideal venting P=0 along the remaining two edges of $y = -\frac{b}{2}$,

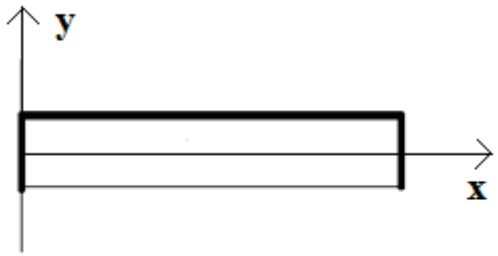

Figure 4.14: The micro-cantilever with three edges closed and venting along the *y* axis

The eigenfunctions is:

$$u_{mn}(x, y) = \sqrt{\frac{2}{ab}} cos \frac{n\pi}{2b}\left(y + \frac{b}{2}\right) \quad (4.44)$$

Here *cos* is used for *n = odd*. The associated eigenvalues are

$$k_{mn} = \frac{n^2\pi^2}{4b^2} \quad (4.45)$$

The normalized pressure distribution for this kind of plate can be derived as

$$P = \sum_{n=odd} \frac{4x^2}{\pi n L^2} \frac{-j\omega H' e^{j\omega t}}{j\omega + k^2{}_{mn}/a^2} (-1)^{\frac{n-1}{2}} \times \cos\frac{n\pi}{2b}\left(y + \frac{b}{2}\right) \tag{4.46}$$

The concentrated force at the tip of the plate can be expressed as:

$$F(t) = \sum_{n=odd} Pa \frac{-jwH' e^{j\omega t}}{j\omega + k^2{}_{mn}/a^2} * \frac{8ab}{5*\pi^2 n^2} \tag{4.47}$$

The air stiffness and air damping can be found from the force function. Then the simulated and analytical frequency responses can be compared..

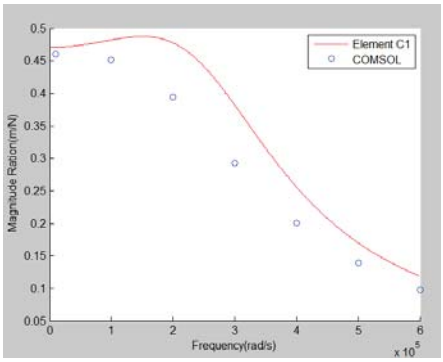

Figure 4.15: Regular cantilever 'C1' with three edges closed and venting along the y axis

The simulated result and analytical result match well as shown in Figure 4.15, thus demonstrating that the analytical model of regular cantilever 'C1' works.

Then we can start to derive the analytical model of element 'C1' shown in Figure 4.7. The domain of the volume is taken to be $a_1 \leq x \leq a_2$ and $b_1 \leq y \leq b_2$, corresponding to a rectangular plate of dimensions $a \times b$, where $a = a_2\text{-}a_1$ and $b = b_2\text{-}b_1$. Plate 'C' has three edges closed but venting along with y axis, the boundary conditions can be expressed as $\frac{\partial P}{\partial y} = 0$ at $y = b_1$, and $\frac{\partial P}{\partial x} = 0$ at $x = a_1, a_2$. With venting P=0 along the edge of x=b_2. The eigenfunctions become:

$$u_{mn}(x, y) = \sqrt{\frac{2}{ab}} cos\frac{n\pi}{2b}(y - b_1) \tag{4.48}$$

Here *cos* is used for $n = odd$. The associated eigenvalues are

$$k_{mn} = \frac{n^2\pi^2}{4b^2} \tag{4.49}$$

The normalized pressure distribution for this kind of plate can be derived as

$$P(x, y, t) = \sum_{n=odd} \frac{4x^2}{\pi n L^2} \frac{-j\omega H' e^{j\omega t}}{j\omega + k^2{}_{mn}/a^2} (-1)^{\frac{n-1}{2}} \cos\frac{n\pi}{2b}(y - b1) \tag{4.50}$$

The concentrated force at the tip of the plate can be expressed as:

$$F(t) = P_a \int_{a_1}^{a_2} \int_{b_1}^{b_2} (\frac{x}{L})^2 P(x,y,t) dxdy$$
$$= \sum_{n=odd} \frac{8a^5 * b}{5\pi^2 n^2 L^4} \frac{-j\omega H' e^{j\omega t}}{j\omega + k^2{}_{mn}/a^2} \quad (4.51)$$

The stiffness of air underneath cantilever is the spring component of the reaction force divided by the tip displacement.

$$k_{spring} = F(t)/H'$$
$$= Re[\sum_{n=odd} \frac{8a^5 * b}{5\pi^2 n^2 L^4} \frac{-j\omega H' e^{j\omega t}}{j\omega + k^2{}_{mn}/a^2}] \quad (4.52)$$

Similarly, the damping coefficient of air underneath cantilever can be determined from the damping component of the reaction force divided by the tip velocity:

$$b_{damping} = F(t)/v$$
$$= Im[\sum_{n=odd} \frac{8a^5 * b}{5\pi^2 n^2 L^4} \frac{-j\omega e^{j\omega t}}{j\omega + k^2{}_{mn}/a^2}] \quad (4.53)$$

4.2.5 Plate 'C2' with three edges closed but venting along the *x* axis

The derivation begins with the equation for the regular cantilever with three edges closed but venting along the *x* axis as shown in Figure 4.16. The boundary conditions for three edges closed but venting along with *x* axis are expressed as $\frac{\partial P}{\partial x} = 0$ at $x = 0$, and $\frac{\partial P}{\partial y} = 0$ at $y = \frac{b}{2}$, $y = -\frac{b}{2}$. With ideal venting $P=0$ along the remaining two edges of $x = a$,

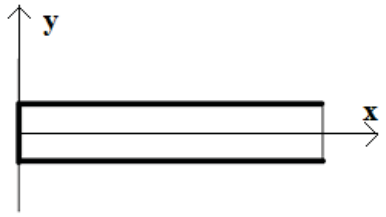

Figure 4.16: The micro-cantilever with three edges closed and venting along the *x* axis

The eigenfunction is:

$$u_{mn}(x,y) = \sqrt{\frac{2}{ab}} cos \frac{n\pi}{2a}(x) \quad (4.54)$$

Here *cos* is used for *n= odd*. The associated eigenvalues is:

$$k_{mn} = \frac{n^2\pi^2}{4a^2} \quad (4.55)$$

The normalized pressure distribution for this kind of plate can be derived as

$$P(x,y,t) = \sum_{n=odd} \frac{4}{\pi^3 n^3} \frac{-j\omega H' e^{j\omega t}}{j\omega + k^2{}_n/a^2} (\pi^2 n^2 - 8)(-1)^{\frac{n-1}{2}} \times \cos\frac{m\pi}{2a}(x) \quad (4.56)$$

The concentrated force at the tip of the plate can be expressed as:

$$F(t) = Pa(\sum_{n=odd} \frac{8ab}{\pi^6 n^6} \frac{-j\omega H' e^{j\omega t}}{j\omega + k^2{}_n/a^2} (\pi^2 n^2 - 8)^2) \quad (4.57)$$

The air stiffness and air damping can be known using force function. Then compared the simulate result with analytical result using magnitude ratio.

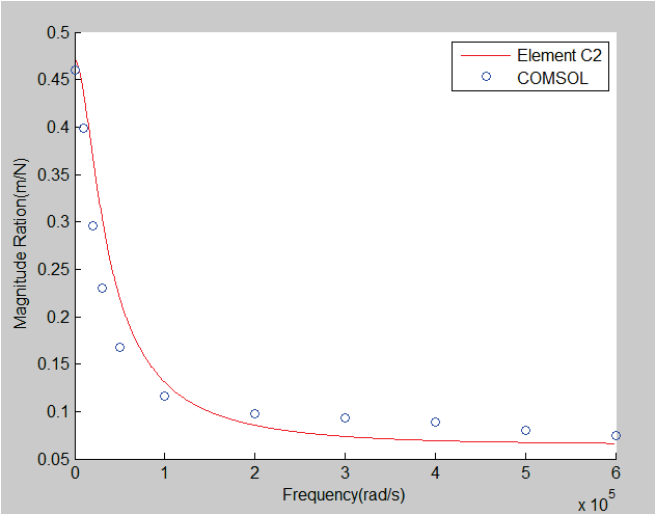

Figure 4.17: Regular cantilever 'C1' with three edges closed and venting along the x axis

The simulated result and analytical result match well as shown in Figure 4.17, thus demonstrating that the analytical model of regular cantilever 'C2' works.

Then we can start to derive the analytical model of element 'C2' showed in Figure 4.7. The domain of the volume is taken to be $a_1 \leq x \leq a_2$ and $b_1 \leq y \leq b_2$, corresponding to a rectangular plate of dimensions $a \times b$, where $a = a_2 - a_1$ and $b = b_2 - b_1$. Plate 'C2' has three edges closed but venting along with x axis, the boundary conditions can be expressed as $\frac{\partial P}{\partial y} = 0$ at $y = b_1, b_2$ and $\frac{\partial P}{\partial x} = 0$ at $x = a_1$. With venting $P=0$ along the edge of $x = a_2$. According to these boundary conditions, the eigenfunctions become:

$$u_{mn}(x,y) = \sqrt{\frac{2}{ab}} \cos\frac{m\pi}{2a}(x - a_1) \quad (4.58)$$

Where $m = \{1,3,5\ldots..\}$. The associated eigenvalues are

$$k_{mn} = \frac{m^2\pi^2}{4a^2} \quad (4.59)$$

Following the approach described in Darling's paper, the normalized pressure distribution for this kind of plate can be derived as

$$P(x,y,t) = \sum_{m=odd} \frac{4}{\pi^3 m^3 L^2} \frac{-j\omega H' e^{j\omega t}}{j\omega + k^2_{mn}/a^2} \left((\pi^2 \mathrm{m}^2 {a_2}^2 - 8\mathrm{a}^2)(-1)^{\frac{m-1}{2}} - 4\pi a m a_1 \right) * \cos\frac{m\pi}{2a}(x - a_1) \quad (4.60)$$

Following the approach in Darling's paper, the concentrated force at the tip of the plate can be computed as:

$$F(t) = P_a \int_{a_1}^{a_2} \int_{b_1}^{b_2} (\frac{x}{L})^2 P(x,y,t) dx dy$$

$$= \sum_{m=odd} Pa \frac{-j\omega H' e^{j\omega t}}{j\omega + k^2_{mn}/a^2} * \frac{8\mathrm{ab}}{\pi^6 m^6 L^4} * \left((\pi^2 \mathrm{m}^2 {a_2}^2 - 8\mathrm{a}^2)(-1)^{\frac{m-1}{2}} - 4\pi a m a_1 \right)^2 \quad (4.61)$$

The stiffness of air underneath cantilever is the spring component of the reaction force divided by the tip displacement.

$$k_{spring} = F(t)/H'$$

$$= Re[\sum_{m=odd} Pa \frac{-j\omega e^{j\omega t}}{j\omega + k^2_{mn}/a^2} * \frac{8\mathrm{ab}}{\pi^6 m^6 L^4} * \left((\pi^2 \mathrm{m}^2 {a_2}^2 - 8\mathrm{a}^2)(-1)^{\frac{m-1}{2}} - 4\pi a m a_1 \right)^2] \quad (4.62)$$

Similarly, the damping coefficient of air underneath cantilever can be determined from the damping component of the reaction force divided by the tip velocity:

$$b_{damping} = F(t)/v$$

$$= Im[\sum_{m=odd} Pa \frac{-je^{j\omega t}}{j\omega + k^2_{mn}/a^2} * \frac{8\mathrm{ab}}{\pi^6 m^6 L^4} * \left((\pi^2 \mathrm{m}^2 {a_2}^2 - 8\mathrm{a}^2)(-1)^{\frac{m-1}{2}} - 4\pi a m a_1 \right)^2] \quad (4.63)$$

4.3 Comparison of the pressure between analytical model and COMSOL model

For the cantilever with a hole in the center, COMSOL and analytical models were used to compare the damping pressure at several points. The damping pressure of analytical model can be calculated according by the each element equation with the parameters showed in Table 4.2.

Table 4. 2: Parameter used in cantilever with a hole in the center

Pa	101000 Pa
$\mu_{effective}$	1.862×10^{-5} Pa.s
L	300 μm
W	100 μm
t	3 μm
ρ	2330 kg/m^3
g_0	4 μm
s (hole size)	50 μm × 50 μm

Figure 4.18 is showing the air damping pressure distribution in cantilever with a hole in the center. The hole in the center is using Boolean Operations by subtracting the rectangular cantilever and square plate so that this model is one element. The red area represents the high air damping pressure, and the air damping pressure in the blue area is small. This pressure distribution is reasonable, because the area close to the free edge goes large displacement, which means the air underneath was compressed more. This model is close to the realty.

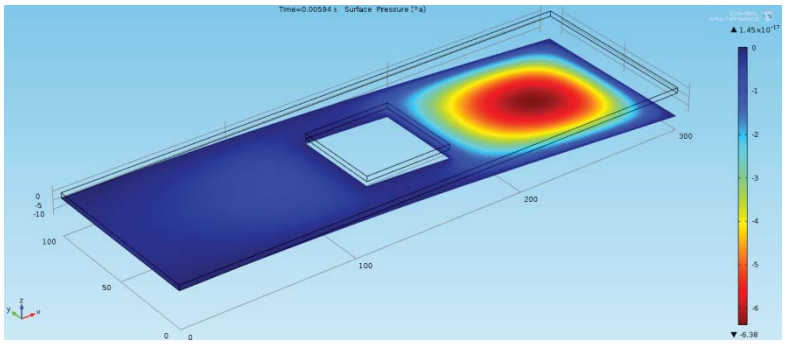

Figure 4.18: Pressure distribution in one element COMSOL cantilever model

The air damping pressure of several points on each element in COMSOL model and analytical model are compared at the frequency of 10000rads/s. This frequency is at the very beginning of the frequency response, which means it has the lowest difference in pressure compared to at other frequencies.

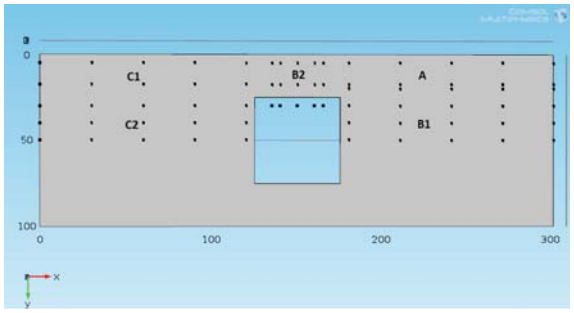

Figure 4.19: Points used to compare the damping pressure between analytical and COMSOL

Figure 4.20 shows the pressure comparison at element 'A', element 'B2' and element 'C1'. They are dependent on the x and y coordinates. The differences between analytical and COMSOL are large even though this model is oscillating at 10000 rads/s, which is a very low frequency. The pressures on element 'A' and element 'B2' increase with x because of the increasing displacement along x axis. The analytical pressure of element 'C1' also increases with x. The COMSOL pressure goes down at the end of element 'C1' because of the hole. The air can flow out from the hole and thus reduce the damping pressure.

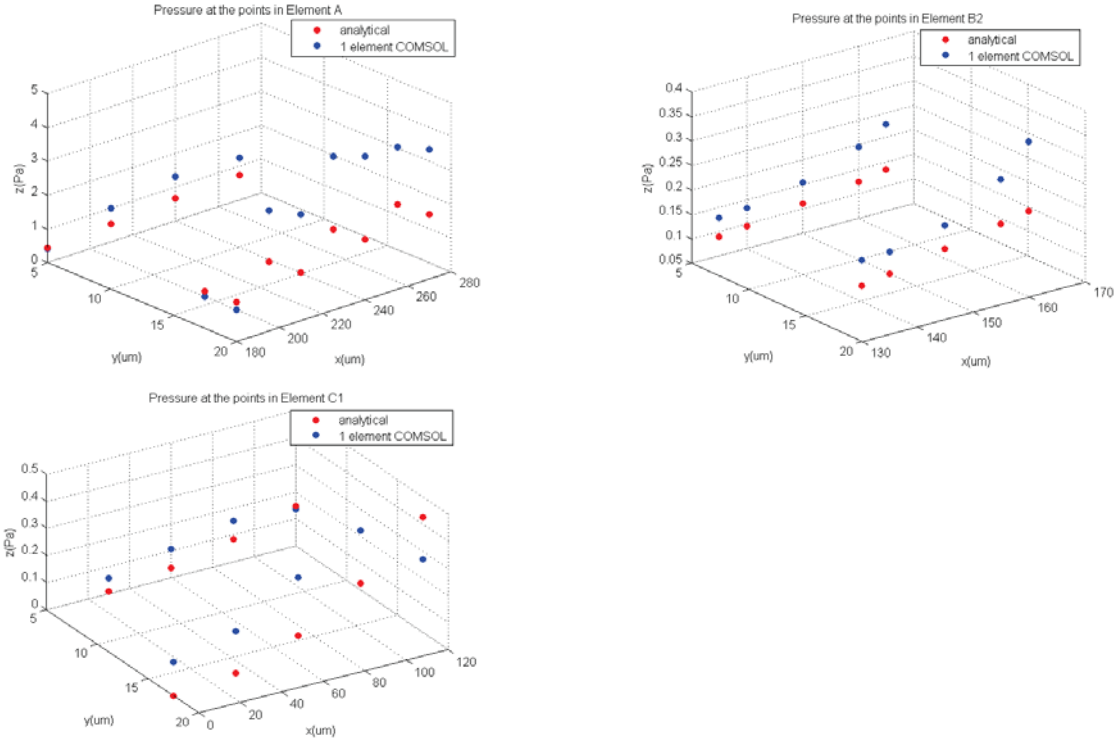

Figure 4.20: Pressure comparison between COMSOL and analytical.

Figure 4.21 compared the air damping pressure of several points on element ‘B1’ and element ‘C2’. Analytical model shows that the damping pressure will not change by y axis, because the analytical boundary conditions of element ‘B1’ and element ‘C2’ are symmetric about x axis. But the pressure of COMSOL will changed along y axis. The points closer to the middle line of cantilever model, the larger distance from the edge.

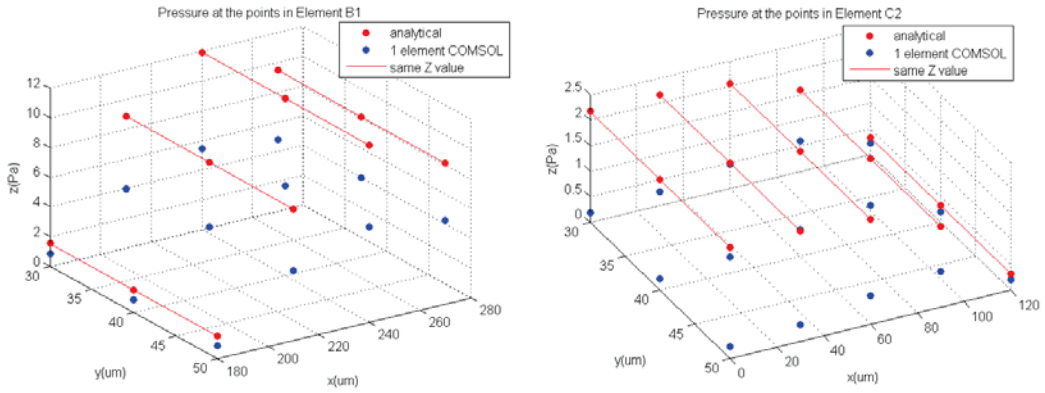

Figure 4.21: Pressure comparison between COMSOL and analytical

The comparison above indicates that the analytical model does not match reality. There are two reasons for these results, the first is the boundary conditions assumption. The air underneath the cantilever can cross each edge in the real life, but the boundary conditions of analytical model prohibit the air cross the closed edges. Secondly, the deflection shape function of cantilever. The analytical shape function is $\frac{x^2}{L^2}$ in previous analytical model, but this equation is the simplest way to describe the bending shape in cantilever. Some more models need to be compared.

4.4 Investigation of the boundary condition assumptions

The same micro-cantilever was modeled in COMSOL with the parameters shown in Table 4.2. The cantilever was divided into 8 small plates with five kinds of elements in total. The COMSOL model was adjusted to mimic the analytical model in terms of the boundary conditions. For example, Element 'A' has two adjacent edges closed, Element 'B1' has two opposite edges closed along the y axis and element 'B2' has two opposite edges closed along the x axis. Element 'C1' has three edges closed but venting along the y axis, element 'C2' has three edges closed but venting along the x axis. A narrow element with a width of 0.1 μm was used to separate neighboring elements, and the damping on these narrow elements was set to zero. This creates a "wall" between elements that has the same effect as the analytical boundary conditions shown in Figure 4.22. A sinusoidal edge load $1 \times 10^{-2} \times \sin(\omega \times t)$ *N/m* is applied at the free edge of the cantilever. Several points at the bottom surface of cantilever are created. The damping pressures at these points were found for different input frequencies.

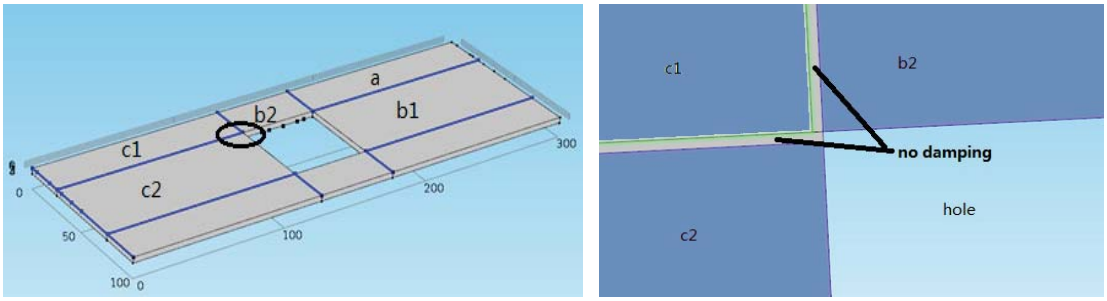

Figure 4.22: Cantilever with a hole in the center in COMSOL

Figure 4.23 shows the air damping pressure distribution in cantilever with a hole in the center. The pressure distribution is not as smooth as the first model. This model is close to the analytical model, but not reality.

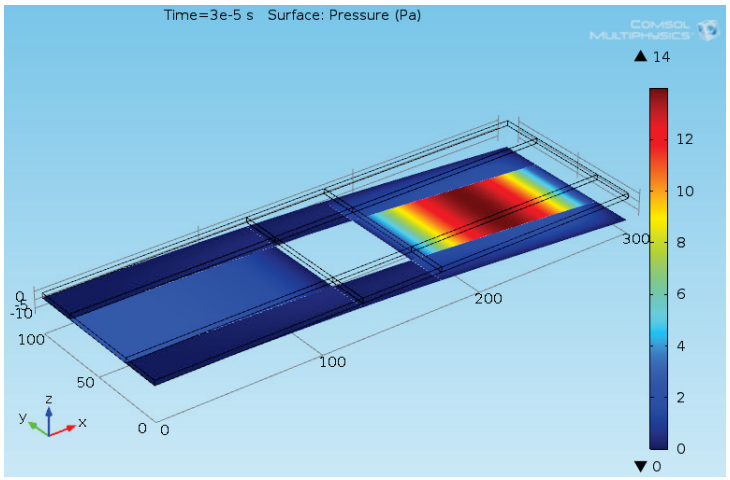

Figure 4.23: Pressure distribution in eight elements cantilever model

For a very low frequency of 10000rads/s, Figure 4.24 shows the damping pressure of the three elements ‘C1’, ‘B2’ and ‘A’. They all change with x and y. Element ‘B1’ has the large damping pressure (about 10 Pa) and small difference (about 20%) compared to the other elements. It is because the element ‘B1’ is close to the free edge so that it has the highest compressional displacement and its own boundary condition. Element ‘C1’ and element ‘B2’ have smaller damping pressures. The pressures decrease toward the venting edge in the y axis and increase along the x axis because of increasing compression.

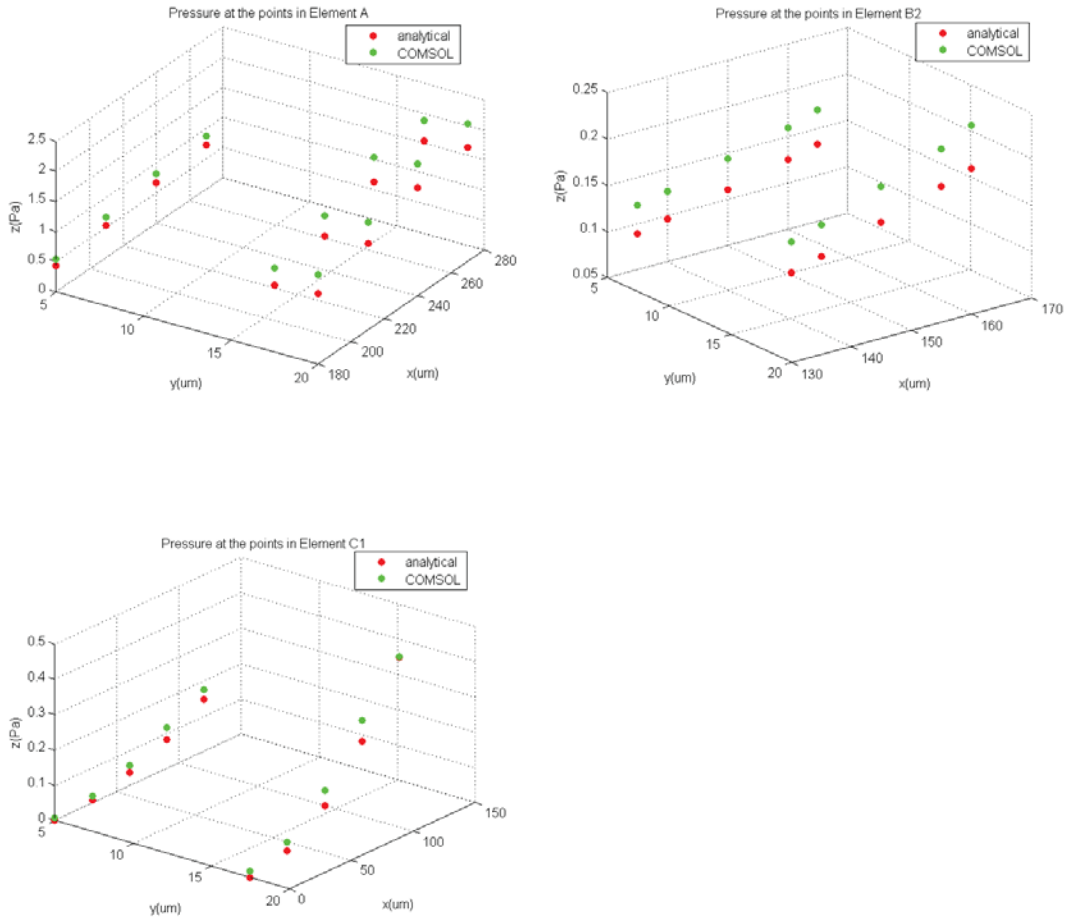

Figure 4.24: Pressure comparison between analytical model and COMSOL model with boundary walls

Figure 4.25 shows that the damping pressure on element 'C2' and element 'B1' are independent of y axis, which is reasonable because these two elements are symmetric about the x axis.

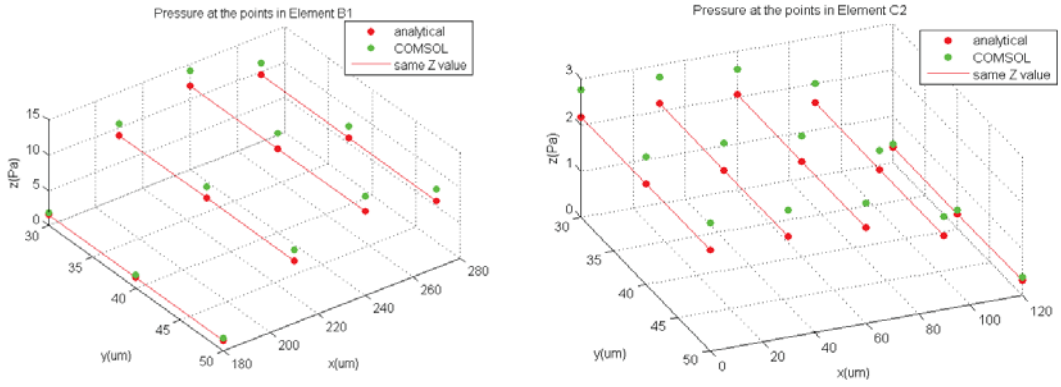

Figure 4.25: Pressure comparison between analytical and COMSOL model

These results indicate that the analytical model and the COMSOL model with walls match fairly well. The difference is up to 20%. This COMSOL model is not a realistic model because of the boundary conditions. The closeness of the analytical and COMSOL pressures demonstrates that the boundary condition assumptions that worked well for other geometries cause a problem in the model of cantilever with a hole in the center.

4.5 Investigation of the deflection function

The deflection of the cantilever is approximated as $\frac{x^2}{L^2}$ in Darling's paper. This assumption is different from the real analytical function. Because of the concentrated load applied at the free end of cantilever in COMSOL simulated model, the analytical deflection equation can be found.

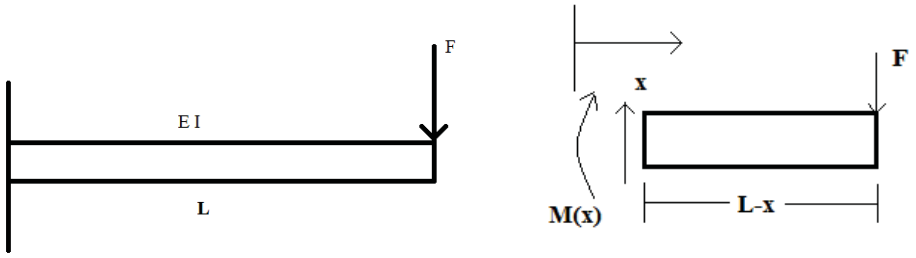

Figure 4.26: Free body diagram of cantilever with a concentrated load at free edge

Figure 4.26 shows the deflection model, The moment and curvature equations are:

$$M(x) = -F * (L - x) \tag{4.64}$$

$$E * I * V\ddot{(x)} = M(x) = -F * (L - x) \tag{4.65}$$

Integrating twice to find the displacement V in the y direction produces:

$$E * I * \dot{V(x)} = \int -F * (L - x)\, dx$$

$$= -F * \left(Lx - \frac{x^2}{2}\right) + C_1 \tag{4.66}$$

$$E * I * V(x) = \int -F * \left(Lx - \frac{x^2}{2}\right) dx + C_1 x + C_2 \tag{4.67}$$

The boundary condition of the cantilever is $\frac{dV}{dx}(0) = 0, V(0) = 0.$

C1=0, C2=0.

The boundary conditions of the cantilever are $\frac{dV}{dx}(0) = 0, V(0) = 0.$ From these, the integration constants are:

$$E * I * V(x) = \int -F * \left(Lx - \frac{x^2}{2}\right) dx = -F * (\frac{Lx^2}{2} - \frac{x^3}{6})$$

$$abs(V(x)) = \frac{Fx^2}{6EI} * (3L - x)$$

$$abs(V(tip)) = V(L) = \frac{FL^3}{3EI}$$

$$V(x) = \frac{1}{2}\left(\frac{3x^2}{L^2} - \frac{x^3}{L^3}\right) * V(tip) \tag{4.68}$$

Figure 4.27 compares the cantilever displacements between COMSOL, simple approximate $\frac{x^2}{L^2}$ and polynomial approximation $\frac{1}{2}\left(\frac{3x^2}{L^2} - \frac{x^3}{L^3}\right)$. The cantilever is 300 $\mu m \times$ 100μm with a 0.01 N/m load applied at the free end edge. The polynomial approximation plot goes through all the COMSOL results. The difference between these two results is between -1.12% to 1.92%. The difference between COMSOL and the $\frac{x^2}{L^2}$ model result is almost 20%. This demonstrates that the polynomial equation gives a very good approximation of the cantilever deflection that is much better than the simple approximation..

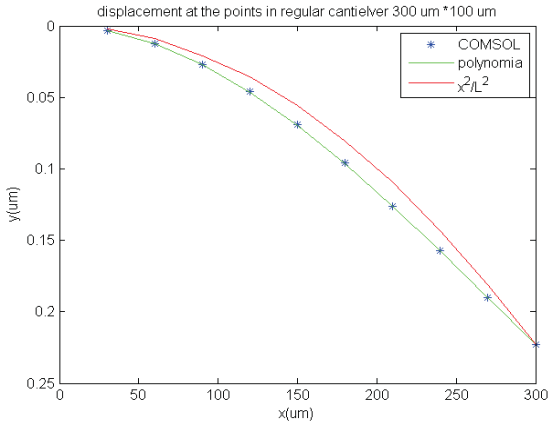

Figure 4.27: Compare the deflection shape between COMSOL and two analytical models

4.6 Pressure comparisons with different deflection equations

The boundary conditions for the one edge closed cantilever are expressed as $\frac{\partial P}{\partial x} = 0$ at x = 0, with ideal venting P=0 along the other three edges. The eigenfunction is expressed as:

$$u_{mn}(x,y) = \sqrt{\frac{4}{ab}} cos\frac{m\pi}{2a}(x) \times \cos\frac{n\pi}{b}(y) \tag{4.69}$$

Where *cos* is used for *m*, *n* = odd; The associated eigenvalues are

$$k_{mn} = \frac{m^2\pi^2}{4a^2} + \frac{n^2\pi^2}{b^2} \tag{4.70}$$

The normalized displacement of the plate can be described as

$$H(x,y,t) = \frac{1}{2}(\frac{3x^2}{L^2} - \frac{x^3}{L^3})H^{'}e^{jwt} \tag{4.71}$$

Where L is the length of the cantilever and $H^{'}$ is the maximum displacement at the free end. The normalized pressure distribution for this kind of plate can be derived as

$$P(x,y,t) = \sum_{n=odd} \frac{16}{\pi^5 m^4 n} \frac{-j\omega H' e^{j\omega t}}{j\omega + {k^2}_n/a^2} \left((\pi^3 m^3)(-1)^{\frac{m-1}{2}} - 24\right)(-1)^{\frac{m-1}{2}} \times \cos\frac{m\pi x}{2L} \times cos\frac{n\pi y}{W} \tag{4.72}$$

The concentrated force at the tip of the plate can be computed as:

$$F(t) = \sum_{n=odd} Pa \frac{-j\omega H' e^{j\omega t}}{j\omega + \frac{k^2 n}{a^2}} * \frac{64\mathrm{WL}}{\pi^{10} m^8 n^2} * \left((\pi^3 m^3)(-1)^{\frac{m-1}{2}} - 24\right)^2 \tag{4.73}$$

Figure 4.28 compares the damping pressures of the analytical model using the two different deflection equations to COMSOL. The cantilever is $300\mu m \times 50um \times 3um$. A load of $1 \times 10^{-2} \times \sin(\omega \times t)$ *N/m* is applied at the free end edge. Figure 4.27 shows the pressures for a frequency of 10000 rad/s. The polynomial results are closer to COMSOL results; the difference between these two models is almost around 11%. The difference between COMSOL and the analytical model with the simple deflection approximation $\frac{x^2}{L^2}$ is almost 25%.

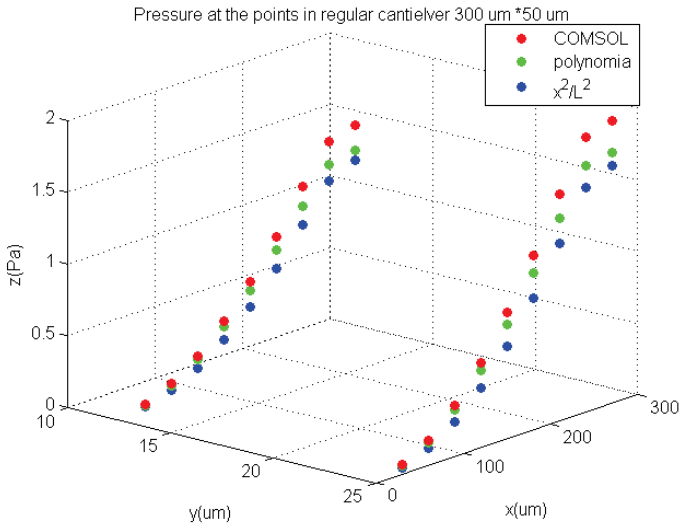

Figure 4.28: Pressure comparison between COMSOL and two analytical models

This figure demonstrates that the deflection function influences the damping pressure. There is no doubt to say that the deflection equation $\frac{x^2}{L^2}$ is one of the reasons that explains why the damping pressure is different in the model of cantilever with a hole in the center.

4.7 Optimization of micro-cantilever by COMSOL

The vapor sensor is covered by a chemical coating, which is used to absorb the particular chemical vapor molecules. The mass of the cantilever will increase due to the absorbed chemical vapor. The goal is find the optimum hole size which has low air damping force and large chemical coating area for absorbing the chemical vapor. Following the parameter Q_s defined by Miller and Li [21], which is just need two points of the root mean square deviation (RMSD) measurement. It is expressed as below:

$$Q_S = \sqrt{\frac{(M_{ab}^r - M_{no})^2 + (M_{no}^r - M_{ab})^2}{(M_{no})^2 + (M_{ab})^2}} \times 100\% \qquad (4.74)$$

Where M_{ab}^{r} and M_{no}^{r} are the magnitude ratio at the resonant frequencies of the absorbed mass system and without absorb system, respectively. Figure 4.29 shows the frequency responses for two different systems with and without absorb chemical vapor mass. And also shows the parameters in the previous equation.

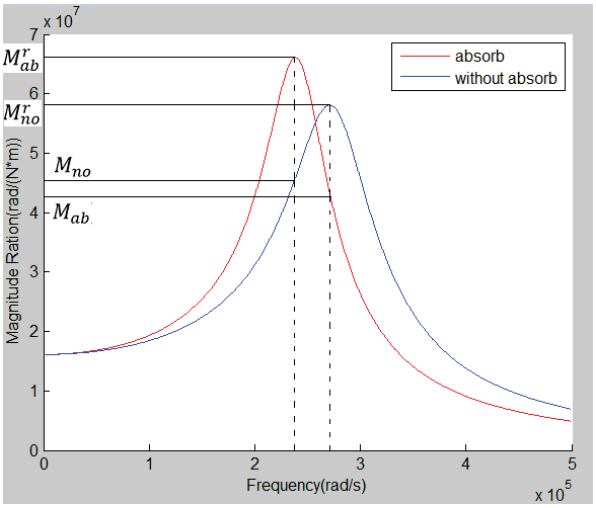

Figure 4. 29: The parameter definitions of Q_S

The cantilever is coated with a polymer chemical coating that will absorb the particular chemical vapor. For example, in [17], the plate is coated by PPEOsNa+ polymer to absorb nerve gas analog (DMMP). The DMMP will be absorbed approximately 5.6 mg/m^2 by 100 *nm* thick polymer coating. Because the coating area corresponds to the cantilever area, in this case, I assume that the absorbed chemical vapor adds 10% to the mass of the plate. This thesis is focus on how the hole size will influence the Qs of cantilever. The table 4.3 below shows the parameters that used in the optimization design of cantilever by COMSOL.

Table 4. 3: Parameters used in COMSOL cantilever model

Pa	101000 Pa
μ	2.26×10^{-5} Pa.s
L	300 μm
W	100 μm
t	3 μm
ρ	2330 kg/m^3
g_0	4 μm
k_{flex}	Calculated by COMSOL Automatically
$b_{material}$	Calculated by COMSOL Automatically

The steps for creating a COMSOL model and got the Q_S value were as follows:

1. Sketch a cantilever with a hole in the center in COMSOL MULTIPHYSICS as show in Figure 4.19 using the parameters in Table 4.3.
2. Choose the solid mechanics physics and eigenfrequency model.
3. Set the thin-film damping on the bottom surface of the cantilever with a gap of 4 um, the ambient pressure is 1 atmospheric pressure and the viscosity of air is $22.6 \times 10^{-6}\ Pa.s$ in a room temperature of 293.15 K. The material of the cantilever is silicon.
4. Find the first model of eigenfrequency that is the resonant peak frequency with no absorption as show in Figure 4.29. And record this frequency value.
5. Run the time dependent model. Apply the sinusoidal load $1 \times 10^{-2}\times\sin(\omega\times t)\ N/m$ at the free edge of the cantilever with the frequency of eigenfrequency got last step. M_{no}^{r} shown in Figure 4.29 can be got by collect the maximum displacement value of the free edge.
6. Add 10% mass to the entire cantilever, M_{ab} shown in Figure 4.29 can be got by repeat step 5.
7. Run the eigenfrequency model again to find the resonant peak frequency with 10% mass absorption as show in Figure 4.29. And record this frequency value.
8. Repeat step 5, M_{ab}^{r} shown in Figure 4.29 can be got by collect the maximum displacement value of the free edge.
9. M_{no} can be got by repeat step 5 with no absorption.
10. One point of Q_S value can be got by the equation 4.74.

Figure 4.30 shows how the Q_S change with different hole size of fixed-free cantilever. The highest Q_S is 5.207% with the square hole size of 60 μm.

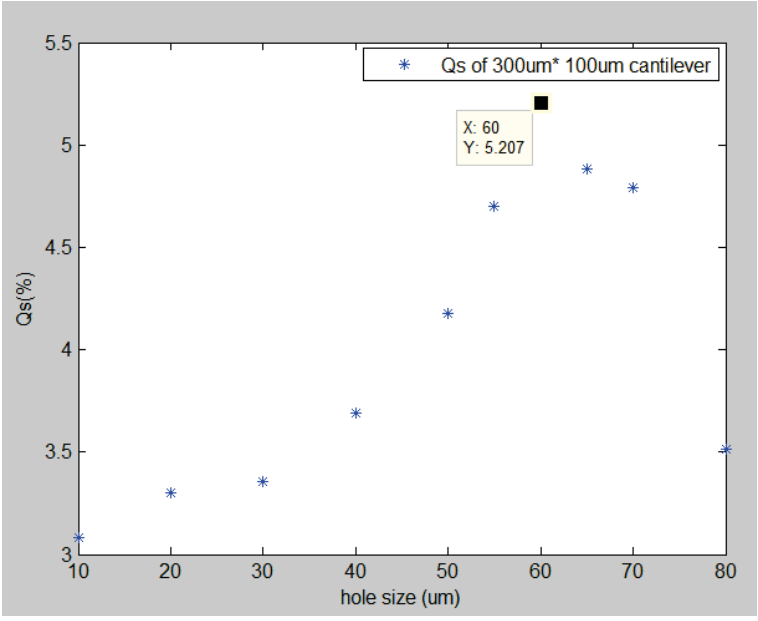

Figure 4. 30: Sensor sensitivity Q_S with different hole size for cantilever based on dx/dF

CHAPTER V Conclusion and Future Work

The ambient pressure, temperature and gap all influence the air damping force. This thesis work keeps these factors as constants while focusing on optimal shape as a way to reduce the air damping. The goal is to build an analytical model and use it to perform design optimization.

This research has developed analytical models of squeeze film damping for three kinds of resonant mass sensor shapes. The first type is a rigid tilting plate about y axis with a hole in the center. Frequency dependent spring constants and damping coefficients of air can be found using a compact squeeze film damping model with appropriate boundary conditions. The *k* and *b* values for multiple elements can be added together to produce models for more complex geometries, such as a tilting plate with a hole. The analytical frequency responses were calculated by a lumped parameter system in MATLAB. To validate the analytical model, COMSOL was used to create simulated frequency responses. The analytical results and simulated results for the tilting plate with hole in the center matched well. The analytical model can be used to find the best hole size that would maximize the resonant mass sensor parameter Q_s, which includes both detectability and sensitivity parameter of sensor. Q_s is a two point RMS calculated from the magnitude ratio at two resonant frequencies with and without absorption. Instead of optimization by finite element method, the analytical model really makes the optimization more efficient.

The second type of resonant mass sensor is a rigid tilting plate that rotates about its diagonal. The same modeling approach was used. The frequency responses of analytical model and COMSOL model match very well. The analytical model is subsequently used for design optimization.

The third type of resonant mass sensor is a fixed-free micro-cantilever with a hole in the center. In this case, the frequency responses generated from the analytical and numerical models did not agree. The discrepancy was explored further by comparing the analytical and COMSOL pressures of several points on the cantilever. The comparison showed that the boundary condition assumptions, necessary to derive the analytical model, do not hold up well. Also, the shape of the cantilever deflection changes as the hole size changes; thus, an analytical model would need the added complexity of a variable shape.

The models were used to make comparisons of the tilting plate about y axis, tilting plate about diagonal, and cantilever in terms of Q_s. Comparing the same size tilting plates and same parameters used shown in Table 3.5, with a 10% mass added to the entire surface, the tilting plate about y axis gives the higher Q_s value at 73% versus the tilting plate about diagonal Q_s value of 68%. The reason is that for the same size plate, tilting about diagonal has more damping force than tilting about y axis. The cantilever with a hole in the center shown in Table 4.3 gives Q_s value of 5.2%. It is low because only the mass added near the free edge has a big influence on the resonant frequency shift.

Several possible extensions of this research remain as future work:

1. For both rigid tilting plates, the analytical models of squeeze film damping focus on a square hole in the center. Additional work needs to be done for changing the location of the hole, the shape of the hole such as circle, hexagon and also multiple holes.

2. For micro-cantilever, some new boundary condition elements need to be created that better approximate realistic flow conditions.

3. With a viable analytical model, the effects of multiple holes and different locations of holes can be explored in order to achieve more optimal designs.

4. For the tilting plate and micro-cantilever designs, the analytical capacitance-actuation equation needs to be simplified, so that electrostatic actuation and capacitive sensing can be included in the model (thus $\frac{dC}{dV}$ can be calculated in addition to dx/dF).

References

[1] M. Bernardine Dias, October 2000, “Investigating the Viability of MEMS Vapor Sensors for Detecting Land Mines”, Carnegie Mellon University.

[2] F. Zee and J.W. Judy, August 2001, “Micromachined polymer-based chemical gas sensor array” Sensor and Actuators, B72, pp. 120-128.

[3]] S. Semancik, R.E. Cavicchi, M.C. Wheeler, J.E. Tiffany, G.E. Poirier, R.M. Walton, J.S. Suehle, B. Panchapakesan, D.L. DeVoe, 2001, “Microhotplate platforms for chemical sensor research” Sensor and Actuators, B77, pp. 579-591.

[4] J. Gong, Q. Chen, W. Fei, S. Seal, 2004, “Micromachined nanocrystalline SnO_2 chemical gas sensors for electronic nose” Sensor and Actuators, B102, pp. 117-125.

[5] F.M. Battiston, J.P. Ramseyer, H.P. Lang, M.K. Baller, 2001, M.K. Baller, Ch. Gerber, J.K Gimzewski, E. Meyer, H.J. Guntherodt “A chemical sensor based on a microfabricated cantilever array with simultaneous resonance-frequency and bending readout” Sensor and Actuators, B77, pp.122-131.

[6] F.M. Battiston, J.P. Ramseyer, H.P. Lang, M.K. Baller, 2001, M.K. Baller, Ch. Gerber, J.K Gimzewski, E. Meyer, H.J. Guntherodt “A chemical sensor based on a microfabricated cantilever array with simultaneous resonance-frequency and bending readout” Sensor and Actuators, B77, pp.122-131.

[7] D.R. Baselt, B. Fruhberger, E. Klaassen, S. Cemalovic, C.L. Britton Jr, S.V. Patel, T.E. Mlsna, D. McCorkle, B. Warmack, 2003, “ Design and performance of a microcantilever-based hydrogen sensor” Sensors and Actuators, B 88, pp. 120-131.

[8] W. Newell, 1968, Miniaturization of tuning forks, Science 161, pp. 1320-1326.

[9] M. Bao, H, Yang, 2007, “Squeeze film air damping in MEMS” Sensors and Actuators, A 136, pp 3-27

[10] S. Vemuri, G.K. Fedder, T. Mukherjee, 2000, “Low-order squeeze film model of simulation of MEMS devices”, Sensors and Actuators, March 27-29, pp. 205-8.

[11] S S Mohite, H. Kesari, V R Sonti, R. Pratap, 2005, “Analytical solutions for the stiffness and damping coefficients of squeeze films in MEMS devices with perforated back plates”. Journal of Micromechanics and Microengineering, 15, 2083–2092.

[12] E.S. Kim, Y.H. Cho, M.U. Kim, “Effect of holes and edges on the squeeze film damping of perforated micromechanical structures”, Korea Advanced Institute of Science and Technology.

[13] A. Pursula, P. Raback, S. Lahteenmaki, J Lahdenpera, 2006, “Coupled FEM simulations of accelerometers including nonlinear gas damping with comparison to measurements”. Journal of Micromechanics and Microengineering, 16, 2345–2354.

[14] S. Nigro, L. Pagnotta, M. F. Pantano, 2012, “Analytical and numerical modeling of squeeze-film damping in perforated microstructures”, Microfluid Nanofluid, 12, 971-979.

[15] P. Li, Y. Fang, F. Xu, 2014, “Analytical modeling of squeeze-film damping for perforated circular microplates”, Journal of Sound and Vibration, 333, 2688-2700.

[16] P. Li, Y. Fang, 2015, “An analytical model for squeeze-film damping of perforated torsional microplates resonators”, Sensors, 15, 7388-7411.

[17] C. Li, 2012, “Design and fabrication of resonant gas sensor for high sensitivity in the presence of air damping”, dissertation of PHD in university of Michigan Technological University, Houghton.

[18] K.L Ekinici, Y.T. Yang, M.L Roukes, 2004, “Ultimate limits to inertial mass sensing based upon nanoelectromechanical systems”, J. App. Phys. 95, 2682 (2004).

[19] Yan. W, Chen WQ. “Structural Health Monitoring Using High-Frequency Electromechanical Impedance Signatures” Advances in Civil Engineering. 2010.

[20] M.H. Miller, C. Li, 2013, “Objective Functions for Optimizing Resonant Mass Sensor Performance”, Michigan Technological University, Stanford University.

[21] M.H. Miller, C. Li, 2013, “Objective Functions for Optimizing Resonant Mass Sensor Performance”, Michigan Technological University, Stanford University.

[22] R.B. Darling, C. Hivick, J. Xu, 1998, “Compact analytical modeling of squeeze film damping with arbitrary venting conditions using a Green’s function approach”, Sensors and Actuators A 70 (1998) 32-41